DISSERTATIONES
TECHNOLOGIAE
UNIVERSITATIS
TARTUENSIS
78

IKECHUKWU OFODILE

Fault tolerant attitude control for nanosatellites: ESTCube-2 case

DISSERTATIONES TECHNOLOGIAE UNIVERSITATIS TARTUENSIS
78

DISSERTATIONES TECHNOLOGIAE UNIVERSITATIS TARTUENSIS
78

IKECHUKWU OFODILE

Fault tolerant attitude control for nanosatellites: ESTCube-2 case

UNIVERSITY OF TARTU
Press
1632

This study was carried out at the Institute of Technology, Tartu Observatory and with the Estonian Student Satellite Programme.

Faculty of Science and Technology, University of Tartu, Estonia.

The dissertation was accepted for the commencement of the degree of Doctor of Philosophy in Physical Engineering on 09.01.2024, by the Joint Council of the Doctoral Program of Engineering and Technology of the University of Tartu.

Supervisors: Assoc. Prof. Andris Slavinskis,
Tartu Observatory,
University of Tartu,

Prof. Gholamreza Anbarjafari,
Institute of Technology,
University of Tartu,

Reviewer: Prof. Mart Noorma,
Tartu Observatory,
University of Tartu,

Opponent: Assoc. Prof. Jaan Praks,
Department of Electronics and Nanoengineering,
Aalto University,
Finland

Commencement: February 12, 2024 at 10:15 am., University of Tartu, Institute of Technology, Estonia.

Publication of this thesis is granted by the Institute of Technology, Faculty of Science and Technology, University of Tartu.

ISSN 2228-0855 (print)
ISBN 978-9916-27-457-6 (print)
ISSN 2806-2620 (pdf)
ISBN 978-9916-27-458-3 (pdf)

University of Tartu Press
www.tyk.ee

ABSTRACT

Attitude control contributes largely to the success of any spacecraft mission. This makes the attitude determination and control subsystem (ADCS) a fundamental element in the development of nanosatellites aimed at remote sensing, scientific experiments and exploration objectives. For a complex space mission, meeting stringent requirements of the ADCS demands mitigating failure possibilities and uncertain disturbances, often linked to system faults, actuation saturation, and miscalculation in parameters.

In view of this, previous methodologies proposed solutions for these challenges in spacecraft design and dynamic systems like aerial vehicles. This thesis proposes a computationally less complex approach specifically tailored for nanosatellites, addressing faults, saturation, and uncertainties through a fault-tolerant attitude control architecture. The objective is to ensure asymptotic stability while overcoming these obstacles. The proposed fault tolerant control system incorporates two methods: an Anti-windup compensator and an Adaptive Neuro-Fuzzy Inference System (ANFIS).

The purpose of the anti-windup compensators for nanosatellites is to effectively manage actuator faults and saturation. The anti-windup compensators that have been developed rely on the Linear Matrix Inequality (LMI) approach, a method previously addressed in literature, ensuring both performance and global stability. Improvements to Fault Tolerant Control (FTC) architecture design with the anti-windup compensator involve transitioning from a Single-input-Single-output (SISO) system to a Multi-input-Multi-output (MIMO) system, implemented channel by channel. This approach is versatile, applicable to various dynamic systems such as nanosatellites, UAVs, and other robotic systems.

The developed FTC, equipped with anti-windup compensators, demonstrates through simulation results its effectiveness in mitigating the impact of actuator faults and saturation. Additionally, the thesis outlines the ANFIS controller's design, which tackles challenges related to actuator faults and saturation by combining a neural network loop with a fuzzy logic scheme. Simulation results indicate that this controller effectively handles system responses, albeit requiring slightly more computational power compared to the pure anti-windup structure, particularly during fault and saturation occurrences.

CONTENTS

LIST OF FIGURES

LIST OF TABLES

LIST OF ABBREVIATIONS

ADC	Analogue to Digital Converter
ACS	Attitude Control System
ADCS	Attitude Determination and Control System
ANFIS	Adaptive Neuro-Fuzzy Inference System
ANN	Artificial Neural Network
AW	Anti-Windup
CGP	Cold Gas Propulsion
CDP	Coulomb Drag Propulsion
COM	Communication System
COTS	Commercial Off-The-Shelf
E-sail	Electric Solar Wind Sail
FDD	Fault Detection and Diagnosis
FTC	Fault Tolerant Control
LEO	Low Earth Orbit
LMI	Linear Matrix Inequality
LQR	Linear Quadratic Regulator
MIMO	Multi-input-Multi-output
NN	Neural Network
OBC	On-Board Computer
PB	Plasma Brake
PD	Proportional-Derivative
RL	Reinforcement Learning
RW	Reaction Wheel
SISO	Single-input-Single-output
SMC	Sliding Mode Control
UAV	Unmanned Aerial Vehicle
UKF	Unscented Kalman Filter

LIST OF ORIGINAL PUBLICATIONS

This thesis is based on the following publications:

[I] Ofodile, I., Ofodile-Keku, N., Jemitola, P., Anbarjafari, G., Slavinskis, A. (2021). Integrated Anti-Windup Fault-Tolerant Control Architecture for Optimized Satellite Attitude Stabilization. IEEE Journal on Miniaturization for Air and Space Systems, 2(4), 189-198.

[II] Ofodile, I., Helmi, A., Clapés, A., Avots, E., Peensoo, K. M., Valdma, S. M., Anbarjafari, G. et al. (2019). Action recognition using single-pixel time-of-flight detection. Entropy, 21(4), 414.

[III] Ofodile, I., Teras, H., Slavinskis, A., Anbarjafari, G. (2022, March). Towards an Integrated Fault Tolerant Control for ESTCube-2 Attitude Control System. In 2022 IEEE Aerospace Conference (AERO) (pp. 1-11). IEEE.

[IV] Ofodile, I., Ehrpais, H., Slavinskis, A., Anbarjafari, G. (2019, June). Stabilised LQR control and optimised spin rate control for nanosatellites. In 2019 9th International Conference on Recent Advances in Space Technologies (RAST) (pp. 715-722). IEEE.

Other related publications:

[1] Ofodile, I., Kütt, J., Kivastik, J., Nigol, M. K., Parelo, A., Ilbis, E., Slavinskis, A. et al.(2019, March). ESTCube-2 attitude determination and control: Step towards interplanetary CubeSats. In 2019 IEEE Aerospace Conference (pp. 1-12). IEEE.

[2] Kulkarni, K., Corneanu, C. A., **Ofodile, I.**, Escalera, S., Baro, X., Hyniewska, S., Anbarjafari, G. et al.(2018). Automatic recognition of facial displays of unfelt emotions. IEEE transactions on affective computing, 12(2), 377-390.

[3] Sham, A. H., Aktas, K., Rizhinashvili, D., Kuklianov, D., Alisinanoglu, F., **Ofodile, I.**, Anbarjafari, G. et al. (2022). Ethical AI in facial expression analysis: Racial bias. Signal, Image and Video Processing, 1-8.

Author's contribution

During the time when all publications of this thesis were prepared and written, the author was an active member of the ESTCube-2 attitude determination and control system as well as the iCV research group. The author's contribution to the publications referred to by their Roman numerals is indicated as follows:

[I] Designed the Anti-Windup Fault-Tolerant Control (AW-FTC) Architecture based on ESTCube-2 model; wrote all sections of the paper for harmonization and review by co-authors.

[II] Prepared data needed for neural network training; analysed results; prepared figures and tables; wrote major sections of the text.

[III] Implemented the Adaptive Neuro-Fuzzy Inference System (ANFIS) on MATLAB based on the ESTCube-2 model and integrated with the AW-FTC; gathered information from co-authors; ran simulations; analysed results; wrote the whole text.

[IV] Designed the LQR control and optimised the spin rate control based on previous work by supervisor for the ESTCube-2 model; linearized system model; ran simulations; analysed results; wrote the whole text.

1. INTRODUCTION

1.1. Motivation

Researchers and space explorers are highly intrigued by nanosatellites due to their potential to serve as platforms for exploring space science, research, and propulsion. Increased demand for nanosatellite applications has driven advancements in their design and technologies, aimed at fulfilling diverse mission objectives and specific requirements. Irrespective of such mission objectives, nanosatellites have common systems and subsystems addressing various parts of the spacecraft operations. The Attitude Determination and Control System (ADCS) stands as a critical subsystem directly influencing mission control objectives. Its pivotal role lies in fulfilling various mission objectives through specific requirements. Specifically, the focus on designing the ESTCube-2 ADCS is aimed at meeting distinct mission requirements to achieve the scientific mission objective of demonstrating the low-Earth orbit (LEO) electric solar wind sail (E-sail).

The ESTCube-2 mission is a build up on the ESTCube-1 based on lessons learnt as part of the Estonian Student Satellite Program [6]. The ESTCube-2 nanosatellite was designed to demonstrate technologies for deep interplanetary space mission of CubeSats and nanosatellites [1]. The ESTCube-2 mission aimed to set a baseline for the ESTCube-LuNa concept aimed at bringing the E-sail to the solar wind. Algorithms for attitude determination and control have been previously developed specifically for ESTCube 2, aligning with the objectives of attitude estimation and control to meet the predefined mission requirements. The ESTCube-2 nanosatellite actuators and sensors have been designed and selected in [7, 8] while attitude control schemes have been designed and simulated [9, 10] based on specifications of the actuators.

For the focus of this thesis, the ADCS will deal mainly with attitude control of nanosatellites with actuators faults. Actuators and other physical control systems are susceptible to faults, failures, and saturation, as outlined in various sources [2, 11, 12]. These issues can arise due to limitations in magnitude and/or rate, where the controller might require an output from the actuator that exceeds its capacity to deliver. The actuator saturation usually occurs when the output of the controller can no longer have an effect on the controllable variable leading to a control phenomenon regarded as “windup”. This windup problem usually results in system instability and further degradation in system performance.

When addressing actuator saturation, several methods have been identified, but the most practical involves preventing the occurrence of the “windup” problem. This can be straightforwardly achieved by guaranteeing that the actuator’s capacity exceeds the controller’s demand, ensuring the actuator can manage the required output. Another approach involves designing the control law in such a way that the controller’s demand remains below the actuator’s limit. Both strategies serve

to prevent actuator saturation and mitigate the "windup" issue effectively. A typical situation is considered when the angular momentum of a spacecraft reaction is pegged at 1.5 mNm while the demand from the controller tends to over saturate the wheel beyond that angular momentum. A solution considered for this involves an additional control concept that ensures the controller tackles the windup problem whenever it occurs and while also maintaining stability. This solution can be referred to as Anti-windup (AW) with employment of the Anti-windup compensators. The solution is also considered for fault and failure in actuators. Exploring and designing this control architecture for nanosatellites brought about consideration of other fault tolerant control (FTC) approaches which are discussed further in this thesis.

In the past, certain FTC methods [13–15] have addressed actuator faults within their systems. However, ensuring asymptotic stability and equilibrium state convergence, while important, isn't adequate for space missions. Achieving stability with finite-time attitude maneuvering and precise pointing becomes imperative in this context. In this thesis, the problems of actuator fault and saturation are addressed with employment of AW technique in the spacecraft actuator system. The approach aims to simplify the FTC structure and enhance the efficiency of the attitude control system for typical complex space missions. Based on the experience of developing and operating ESTCube-1 [6, 16], ESTCube-2 aimed to continue in-orbit demonstration of the plasma brake and the electric solar wind sail (E-sail), commonly known as the Coulomb Drag Propulsion (CDP) system [17].

This research is primarily motivated by the necessity to delve into the design of a FTC structure that ensures stabilization within a finite time while keeping computational complexity minimized. Furthermore, it aims to introduce an FTC architecture specifically tailored to accommodate multiple disturbances, actuator faults, and reaction wheel (RW) saturation. This architecture is optimized to fulfill the Attitude Control System (ACS) mission requirements of the ESTCube-2 nanosatellite [8]. The proposed control architecture will guarantee finite-time equilibrium-state convergence for the ESTCube-2 ACS and ensures optimal performance of the RWs even with limited momentum exchange. The AW based FTC architecture will optimize the performance of the RWs during the deployment of the 300 m tether for the demonstration of the Coulomb Drag Propulsion system. The design does not include a fault-detection observer or disturbance observer, which avoids further computational complexities and allows for larger angle manoeuvres with RWs as demonstrated in simulation results.

1.2. Research Aim and Objectives

The research aims to introduce a Fault-Tolerant Attitude Control architecture designed to effectively address and manage issues related to actuator faults, failures, and saturation specifically in nanosatellites, using ESTCube-2 as the model case.

The fault tolerant control (FTC) architecture provides the system with the ability to tolerate certain faults and disturbances without necessarily identifying such fault, to reduce the effect of the computational complexity. The FTC schemes developed here are not only applicable to nanosatellites alone, but can be expanded and applied to larger spacecrafts as well as adapted for other dynamic systems such as aircrafts and UAVs. Inorder to address the aim of the research, the following objectives will be considered;

- Understand the structure of the satellite model to be able to design the Anti-Windup based FTC architecture based on a full order AW compensator design approach
- Develop the full order AW compensator based on design approach given in [18] and expanded for the satellite model.
- Explore the ANFIS design on the satellite model for further learning and adaptive tuning.
- Conduct simulations to validate the effectiveness of the FTC architecture designed for the ESTCube-2 nanosatellite [11].

1.3. Progress in this work

This work studied and discussed the development of control algorithms for the ADCS on board ESTCube-2. The satellite is planned to be launched in the third quarter of 2023 and further works will present in-orbit validation of the ADCS. For the Coulomb drag propulsion test involving the plasma brake deorbiting experiment and the E-Sail interplanetary propulsion, the ESTCube-2 is required to spin up to one rotation per second for tether deployment [IV]. This is also part of previous works on ESTCube-1 demonstrated and simulated [9]. ESTCube-2 is required to maintain precise attitude stabilization for pointing navigation. Given the necessity to design a system that can maintain satellite control requirements during specific mission phases, this thesis was inspired to focus on the Anti-Windup fault-tolerant control architecture [I].

There was the need to consider a machine learning approach in which [II] focused on the research of using machine learning and neural network models for recognition tasks. This work explored the use of recurrent neural network (RNN)with Gated-Recurrent Unit (GRU) cells as baseline, aimed at retaining long-temporal information in order to output a class prediction. This work showed that neural networks can be applied to store states (spacecraft state space) based on learning from the environment and provide a feedback to the network as reward in a reinforcement learning (RL) scheme. This research work formed the bases of the Adaptive Neuro Fuzzy Inference System implementation on the ESTCube-2 FTC architecture given in [III]. While centered on space research, the thesis presents control algorithms applicable across various systems and research areas.

1.4. Thesis Outline

This work comprehensively presents a Fault Tolerant Control architecture for nanosatellites, showcasing modeling and simulation tests using the ESTCube-2 platform.

Chapter 2 provides an overview and background on Fault Tolerant Control and applications to Aircrafts and Nanosatellites and current implementations with specified missions.

Chapter 3 describes the ESTCube-2 Nanosatellite with its mission objectives and system requirements. It provides preliminary requirements for the ADCS design as well as requirements for the successful deployment of tethers for the Coulomb drag propulsion tests.

Chapter 4 describes the mathematical approach to modelling of nanosatellite dynamics with specific actuator models. The Anti-Windup compensator is developed based on previous works and applied to the nominal PD-like controller.

Chapter 5 focuses more on research studies on machine learning algorithms into fault tolerant control, specifiying studies on reinforcement learning. Additionally, Adaptive Neuro-Fuzzy Inference System is modelled based on Fuzzy logic and compared with the AW design.

Finally, a conclusion and summary of the works of these thesis relating to all published works is given to further present an outline for a potential future research in specified areas.

2. BACKGROUND ON FAULT TOLERANT ATTITUDE CONTROL

2.1. Reference Frame

In the realm of aerospace engineering, understanding and defining the position and orientation of objects in space is crucial. This is achieved using reference frames. Reference frames are used to define the position of a point in space. In aerospace applications, reference frames are used for attitude determination defining position and orientation of a body or point mass, as well as of one frame with respect to another. The following reference frames are mostly used in satellite representations.

2.1.1. Earth-Centred Inertial Reference Frame (ECIF)

The Earth-Centred Inertial Reference Frame (ECIF) has its origin at the centre of the Earth. The x-axis of this reference frame points through the point where the vernal equinox (point when the sun's rays cross directly over the Earth's equator and providing nearly equal periods of day and night) and the equatorial plane cross. The z-axis points through the Geographic North pole and the y-axis is the cross product between x and z axis completing the right hand Cartesian coordinate system.

2.1.2. Earth-Centred Earth Fixed Reference Frame (ECEF)

The Earth-Centred Earth Fixed Reference Frame (ECEF) has its origin at the centre of the Earth and is fixed with respect to the surface of the Earth. The x-axis points in the direction towards the intersection between the Greenwich Meridian and the Equator. The z-axis is the direction from the centre of the Earth pointing towards the North pole while the y-axis is the cross product between the x-axis and the z-axis completing the right handed system.

2.1.3. Spacecraft Body Reference Frame (SBRF)

Spacecraft Body Reference Frame (SBRF) has its origin from the centre of mass of the satellite. The x-axis is orthogonal to the z-axis and the y-axis completes the right hand orthogonal coordinate reference system.

2.2. Attitude Parametrization

2.2.1. Direction Cosine Matrix (DCM)

The DCM represents the attitude in a 3×3 transformation matrix. This is described by the vector dot product between two coordinate axes representing the cosine of the deviation in angle.

$$A = \begin{bmatrix} u \cdot x & u \cdot y & u \cdot z \\ v \cdot x & v \cdot y & v \cdot z \\ w \cdot x & w \cdot y & w \cdot z \end{bmatrix} \tag{2.1}$$

This DCM is less common and applicable in space missions for attitude representation considering the computational power in computing nine elements as opposed to the quaternion representation of four elements. This therefore makes the DCM less economical in computation based on processing power of On-Board Computers (OBC). Additionally, DCM depends on the order of rotation which are sometimes controversial with respect to the rotation angles from DCM. The Euler angle and Quaternion further described is more applicable.

2.2.2. Euler Angles

The Euler angle representation describes one coordinate frame to another in three successive rotations. These successive rotations are defined as roll, pitch and yaw, where the roll angle ϕ is a rotation about the x-axis, the pitch angle θ about the y-axis and the yaw angle ψ about the z-axis. The rotation (axis transformation) matrices are defined as follows:

$$R_x = \begin{bmatrix} 1 & 0 & 0 \\ 0 & \cos\phi & \sin\phi \\ 0 & -\sin\phi & \cos\phi \end{bmatrix} \tag{2.2}$$

$$R_y = \begin{bmatrix} \cos\theta & 0 & -\sin\theta \\ 0 & 1 & 0 \\ \sin\theta & 0 & \cos\theta \end{bmatrix} \tag{2.3}$$

$$R_z = \begin{bmatrix} \cos\psi & \sin\psi & 0 \\ -\sin\psi & \cos\psi & 0 \\ 0 & 0 & 1 \end{bmatrix} \tag{2.4}$$

where R_x is the transformation matrix for a fixed point about the x axis. R_y is the transformation matrix for a fixed point about the y axis. R_z is the transformation matrix for a fixed point about the z axis. Therefore the resultant transformation matrix from inertial to body frame is given as

$$R = R_z.R_y.R_x$$

$$R = \begin{bmatrix} \cos\psi & \sin\psi & 0 \\ -\sin\psi & \cos\psi & 0 \\ 0 & 0 & 1 \end{bmatrix} \begin{bmatrix} \cos\theta & 0 & \sin\theta \\ 0 & 1 & 0 \\ -\sin\theta & 0 & \cos\theta \end{bmatrix} \begin{bmatrix} 1 & 0 & 0 \\ 0 & \cos\phi & -\sin\phi \\ 0 & \sin\phi & \cos\phi \end{bmatrix}$$

$$R = \begin{bmatrix} \cos\theta.\cos\psi & \cos\psi.\sin\theta.\sin\phi - \cos\phi.\sin\psi & \cos\psi.\sin\theta.\cos\phi - \sin\phi.\sin\psi \\ \cos\theta.\sin\psi & \sin\psi.\sin\theta.\sin\phi - \cos\phi.\cos\psi & \sin\psi.\sin\theta.\cos\phi - \sin\phi.\cos\psi \\ -\sin\theta & \cos\theta.\sin\phi & \cos\phi.\cos\phi \end{bmatrix} \tag{2.5}$$

2.2.3. Unit Quaternions

Quaternions are referred to as hyper complex numbers and were first introduced by mathematician Rowan Hamilton in the early 19th century and over time have been applied to mechanics solutions. Quaternions are used to express a rotation by a rotational angle about an axis unlike Euler angles which represent rotations by a series of rotations about x, y or z axes. The rotation performed by quaternions are not explicitly about an x, y or z axes. Just like complex numbers, quaternions have basis i, j, k satisfying the following expression

$$i^2 = j^2 = k^2 = -1 = ijk \tag{2.6}$$

Therefore we can define quaternions as follows representing an addition of both scalar and vector component.

$$q = iq_1 + jq_2 + kq_3 + q_0 \tag{2.7}$$

Thus quaternions contain four numbers and for simplicity in expressions, q_0 is the scalar part of the quaternions and the vector component is represented as

$$q_v = iq_1 + jq_2 + kq_3 \tag{2.8}$$

The normalized quaternion is therefore represented as

$$q_0 = cos(\theta/2) \tag{2.9}$$

$$q_v = \hat{e}sin(\theta/2) \tag{2.10}$$

where

- $\hat{e}$ is the rotational axis,
- θ is the angle of rotation.

The author in [19] defined and derived the multiplication of two quaternions in order to obtain the quaternion rotation as follows

$$a \otimes b = a_0 b_0 - a_v b_v + a_0 b_v + b_0 a_v + a \times b \tag{2.11}$$

In recall of complex conjugates, the quaternion complex conjugate can be represented as

$$q^* = q_0 - q_v = q_0 - iq_1 - jq_2 - kq_3 \tag{2.12}$$

Therefore the norm of a quaternion can then be defined easily as

$$\|q\| = \sqrt{q^* \otimes q} \tag{2.13}$$

$$\|q\| = \sqrt{q_0^2 + q_1^2 + q_2^2 + q_3^2} = 1 \tag{2.14}$$

The inverse of a normalized quaternion satisfying the above equation is

$$q^{-1} = q^* \tag{2.15}$$

2.2.4. Quaternion Rotation

In order to obtain the quaternion rotation operator, we make use of the normalized quaternion defined in Equations 2.9 and 2.10. Therefore we express the quaternion as

$$q = q_0 + q_v = cos(\frac{\theta}{2}) + \hat{e}sin(\frac{\theta}{2}) \tag{2.16}$$

and perform quaternion products in order to obtain the rotations.

By defining two quaternions as $p = cos(\frac{\alpha}{2}) + \hat{e}sin(\frac{\alpha}{2})$ and $q = cos(\frac{\beta}{2}) + \hat{e}sin(\frac{\beta}{2})$ we obtain the quaternion product as follows.

$$r = p \otimes q = \left(cos(\frac{\alpha}{2}) + \hat{e}sin(\frac{\alpha}{2}) \right) \otimes \left(cos(\frac{\beta}{2}) + \hat{e}sin(\frac{\beta}{2}) \right) \tag{2.17}$$

$$r = cos\Big(\frac{\alpha+\beta}{2}\Big) + \hat{e}sin\Big(\frac{\alpha+\beta}{2}\Big) = cos(\gamma) + \hat{e}sin(\gamma) \tag{2.18}$$

The product of two quaternions as seen above represents the two consecutive rotations by α and β. Equation 2.19 represents the rotation of a quaternion and a vector v

$$q \otimes v = (q_0 + q_v) \otimes (0 + v) = -q_v \cdot + q_0 v + q \times v \tag{2.19}$$

However, multiplying this expression by the conjugate of the quaternion q^* gives the expression in Equation 2.20 which is a vector and expressed further in the form of direction cosine matrix in Equation 2.21

$$w = q \otimes v \otimes q^* = \left(cos^2\left(\frac{\alpha}{2}\right) - sin^2\left(\frac{\alpha}{2}\right)\right) v + 2(q_v \cdot v)q_v + 2q_0(q_v \times v) \quad (2.20)$$

$$\begin{bmatrix} w_1 \\ w_2 \\ w_3 \end{bmatrix} = \begin{bmatrix} 2{q_0}^2 - 1 + 2{q_1}^2 & 2q_1q_2 - 2q_0q_3 & 2q_1q_3 + 2q_0q_2 \\ 2q_1q_2 + 2q_0q_3 & 2{q_2}^2 - 1 + 2{q_0}^2 & 2q_2q_3 - 2q_0q_1 \\ 2q_1q_3 - 2q_0q_2 & 2q_2q_3 - 2q_0q_1 & 2{q_3}^2 - 1 + 2{q_0}^2 \end{bmatrix} \begin{bmatrix} v_1 \\ v_2 \\ v_3 \end{bmatrix} \quad (2.21)$$

the DCM above can also be defined as a general rotational matrix

$$C = (2{q_0}^2 - 1)v + 2(q.v)q + 2q_0(q \times v) \quad (2.22)$$

2.2.5. Error Quaternion

The error quaternion is defined as the rotational quaternion between two rotations. The error quaternion is obtained by quaternion product of the inverse quaternion representing the desired quaternion of one point to another and the initial quaternion itself, given below

$$q_e = {q^{-1}}_d \otimes q \quad (2.23)$$

$$q_e = \begin{bmatrix} q_{d0} & q_{d1} & -q_{d2} & -q_{d3} \\ -q_{d1} & q_{d0} & q_{d3} & -q_{d2} \\ q_{d2} & -q_{d3} & q_{d0} & -q_{d1} \\ q_{d3} & q_{d2} & q_{d1} & q_{d0} \end{bmatrix} \begin{bmatrix} q_0 \\ q_1 \\ q_2 \\ q_3 \end{bmatrix} \quad (2.24)$$

The quaternion error q_e satisfies the unit quaternion constraint.

2.3. Fault Tolerant Control

Fault Tolerant Control (FTC) has received significant attention in addressing modern control engineering challenges. Advanced control systems are integral to ensuring the safety and consistent performance of contemporary technological systems. This is especially critical in crucial systems like aircraft, spacecraft, and nuclear and chemical power plants, where even minor faults could lead to catastrophic outcomes for the entire system. As a result, there's a need to develop new control approaches and designs capable of managing such malfunctions while preserving overall system performance and stability. These approaches or designs often fall under the umbrella of Fault-Tolerant Control (FTC) Systems.

The existence of redundant systems is a critical component in FTC. Consequently, the various FTC methods essentially represent diverse approaches for implementing and making the most of these available redundant systems. It is

worth noting that while additional redundancies might enhance the fault tolerance of a system, these redundancies inevitably lead to increased complexity. This added complexity can pose challenges in terms of both the physical design and the financial constraints during the implementation phase. The performance of a control system, therefore relies on existing and available control actuators on the system, and special care has to be taken to avoid over working the available and remaining actuators in the event of an actuator fault or failure in order to properly steer the system to safety. Sensor failures are also important to consider as this may lead to inaccurate information and decision making which can affect the safety of the entire system. It is often easier to employ multiple sensors with various methods to increase the overall reliability of the system. More recently, smart sensors and sensor fusion have been adopted in various applications with the aim of self validating the entire sensor estimation system.

In terms of FTC, actuator faults/failures are more difficult to deal with as they are more directly related to the control and behaviour of the system. Therefore this thesis focuses more on the FTC based on actuator faults/failures. This section, will further discuss some FTC techniques and then FTC solutions applied to spacecraft development.

2.3.1. Classification of Fault Tolerant Control System

FTC systems' design typically revolves around two primary approaches, which hinge on how component redundancy is utilized: passive and active FTC methodologies. In the passive system, component failures are thought and assumed to be known whereby the control system considers and takes into account such failure modes while designing the system. In this scenario, if the control system is crafted considering these potential failure modes, it's anticipated that in the event of a component failure, the system will uphold its intended performance as initially designed. The passive FTC system is such that the control system can work under several operating scenarios or component failure modes which must have been considered at the design stage.

In contrast to the passive system, an active FTC system reacts to the system component failures actively by properly reconfiguring its control actions so that the stability/performance of the entire system can still be acceptable [20]. This approach relies mainly on real-time fault detection/diagnosis system which provides information about the status of the system and the working conditions of its components. One main concern in the active FTC system is the limited time to perform a fault detection and diagnosis (FDD) or fault detection and isolation (FDI). This also increases the computational complexity of the entire processing system. An active FTC has the capacity to deal with unforeseen faults and still achieve an optimal performance of the system. Due to the interest in designing a FTC system that has the capacity to guarantee stability as in the passive FTC

and also to ensure performance optimization provided by the attribute of an active FTC, a hybrid FTC system that combines both active and passive have been considered in recent FTC developments.

The drawback of an active FTC system considered is the increased complexity in processing often leading to longer time delay which is mostly considered undesirable in any control system. An excessive time delay in an FDD system has been shown to contribute adversely to the stability and performance of the system [21]. In such a case, a passive FTC can be incorporated to provide the needed stability in the entire system in a hybrid FTC setup which eventually provides both the stability and optimal performance.

2.3.2. Fault Tolerant Control Approaches to Spacecraft Development

In earlier development of FTC, research works had implemented control schemes to deal with disturbances and uncertainties but failed to address fault and failure in system components [22]. Further research works then aimed at not only accommodating faults but also guaranteeing control performance and system stability [23, 24]. These works implemented control methods based on adaptive control, absolute stability theory, control allocation [25] and sliding mode control (SMC) schemes [26]. These control methods, each has it's advantages and preferences towards performance on any particular system and have been implemented as FTC approach for various applications.

Spacecraft attitude control development, has over the years seen increased interest in the use of FTC strategies to keep up with complex missions capable of sensor and actuator fault estimations. For an active FTC approach, magnetic actuation failure was addressed in formation flying of JC2Sat-FF spacecraft [27]. Based on actuator fault observation, an attitude determination and control system (ADCS) fault processing method was developed for the NS-2 satellite ACS [28]. In another formation flying application, an SMC based FTC was developed ensuring global asymptotic stability [29]. Actuator saturation has also been considered in designing an integrated controller that accommodates faults with FTC capability [30]. An FTC system in a recent study was designed with a nominal controller and second order filter-like compensator capable of handling multiple actuator faults and saturation [31]. Additionally, in Amrr et al. [32], an FTC system with a time delay was designed to handle uncertainties, disturbances and time varying actuator faults for a small spacecraft.

The SMC has been observed to perform better and has advantages over other approaches in FTC system relating to spacecraft applications [33]. Lee et al. [34] developed an SMC approach to deal with actuator fault and external disturbances, in which the actuator fault was modelled as an effectiveness decrease of the actuator. The SMC approach usually requires a large control power, in which most actuators based on momentum exchange are limited by saturation, thereby inca-

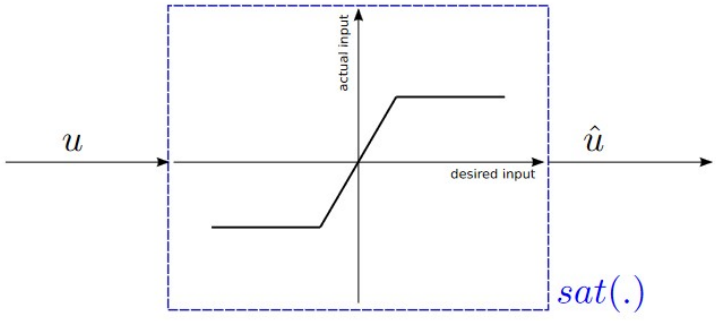

Figure 1. Actuator magnitude saturation non-linearity

pable of providing enough control for required attitude manoeuvre. Due to this limitation, this thesis considers the Anti-Windup (AW) compensator as one alternative to solving problems with failure and saturation in control engineering.

In solving actuator magnitude saturation problems, AW compensator has been designed and applied in combination with feedback controller [35, 36]. An approach previously implemented on a quad-rotor unmanned aerial vehicle, had designed a decentralized AW compensator that guarantees asymptotic stability using linear matrix inequality (LMI) AW synthesis [18, 37]. This approach is re-designed based on the LMIs for the AW synthesis and applied to deal with actuator fault and saturation in the satellite, guaranteeing asymptotic stability and ensuring equilibrium state convergence in finite time.

2.4. Anti-Windup Compensator

A brief description of the "windup" phenomenon is discussed here with a review of Anti-Windup (AW) compensator techniques and methods of synthesis. The idea of the AW compensator considers an actuator in a physical system which is constrained by either magnitude and/or rate limitations. In such a case, saturation occurs in the actuator when the controller demands more than the limits of the actuator and creates a non-linearity in the system. Studies have shown that both magnitude and rate saturation present in a system can significantly impact and affect the stability of the system leading to degraded performance. The non-linearity of the magnitude saturation is represented in Figure 1

The limits of the magnitude saturation are mapped into a range of values and for a scalar case the saturation non-linearity is described by

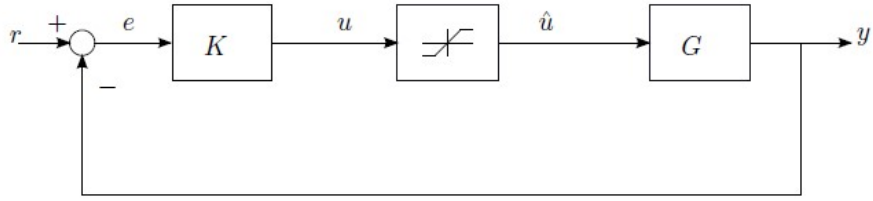

Figure 2. Closed loop control system

$$sat(u), \hat{u} \triangleq \begin{cases} u_N, & \text{if } u \geq u_N \\ u, & \text{if } u_n \leq u \leq u_N \\ u_n, & \text{if } u \geq u_n \end{cases} \tag{2.25}$$

If saturation limits are symmetric then $u_n = -u_N$, where u_n and u_N are the minimum and maximum available actuator values respectively given $sat(.) : \mathbb{R} \longmapsto \mathbb{R}$. Similarly for a vector case given $sat(.) : \mathbb{R}^m \longmapsto \mathbb{R}^m$ with a symmetric non-linear saturation given by

$$sat(u) = [sat(u_1), ..., sat(u_m)]^T$$

where $sat(u_i) := min|u_i|, \bar{u}_i \times sign(u_i)$.

A closed loop control system with a typical PID controller has been observed to encounter the "windup" phenomenon caused by its actuator saturation as shown in Figure 2. In the Figure, u is the unsaturated control signal and $\hat{u} \in \mathbb{R}^m$ is the unsaturated control signal input to the plant y is the plant output, r is the reference input, K is the nominal controller and G is the described plant. Typical actuator saturation and control signal saturation are considered and the "windup" problem has been used to describe any form of performance degradation that could occur. Common effects of the saturation on control systems which may arise from failure of the actuator to meet the demands of the controller are long rise and settling times, change of direction/phase shifts, large overshoots and prolonged periods of actuator saturation. All these may lead to instability in the entire system, therefore giving rise to the need to avoid or prevent the occurrence in practical engineering applications.

Modern Anti-Windup Compensators

Modern AW compensators are based on techniques with earlier generic AW frameworks and eventually graduated to more complex methods. Several modern AW approaches have been discussed in literature and classified on various criteria based on stability and performance objectives [35, 38–40]. Most AW frameworks have a generic structure as shown in Figure 3 where the plants, controllers and AW compensators can either be in a linear or non linear form therefore giving rise to

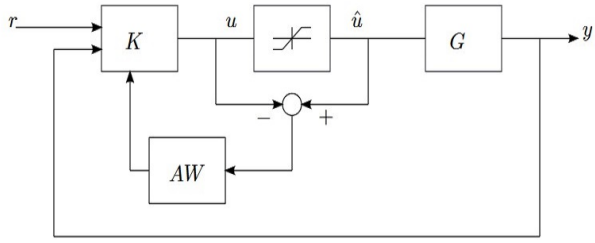

Figure 3. Basic Anti-Windup Structure

various AW formulations. Most AW algorithms are synthesised using Linear Matrix Inequalities (LMI) [41, 42], but there are other synthesis methods using Linear Quadratic Regulators [43] (LQR) and Lyapunov Equation Solution [44, 45]. In view of all the AW frameworks and performance obejctives as well as stability concerns, the approach adopted for the AW design in this work is as described in [18, 46] and discussed further in Chapter 4.3 where a brief description and set up of the AW framework is given.

3. ESTCUBE-2 MISSION OBJECTIVES AND REQUIREMENTS

The ESTCube-2 is a three-unit CubeSat with scientific mission objective of low-Earth orbit technology demonstration. The primary mission objective was to demonstrate the electric solar wind sail (E-sail) in the LEO where the electric sail can be used as an ionospheric plasma brake (PB) for deorbiting. The PB utilizes an induced Coulomb drag effect in the LEO's ionosphere from a charged tether. The tether is charged in synchronization with the satellite spin rate. Further details and experiment requirement of the PB are described by Iakubivskyi et al. [17]. The ESTCube-2 includes other secondary experiments such as the deep-space platform prototype, Earth observation cameras and a material corrosion experiment [1].

The specific requirements for the ESTCube-2 ADCS which stems from the mission objectives as earlier mentioned include the following:

- Spin up the satellite in order to deploy the tether for plasma brake technology demonstration using centrifugal force.
- Obtain attitude measurements for estimating the Coulomb drag effect.
- Provide the angular momentum and spin control for tether deployment.
- Ensure a pointing accuracy of at least $0.25\,\text{deg}$.
- Ensure a pointing stability of $0.125\,\text{deg}/s$.

3.1. Satellite Design

The design of the ESTCube-2 satellite is based on lessons learned from the ESTCube-1 mission [6] ensuring that the PB tether is deployed satisfactorily. The mechanical design of the satellite is done to accommodate an avionics stack, the side panel system and the various payloads. The avionics stack as shown in Figure 4 consists of the on-board computer (OBC) system for data logging, storage and task scheduling; the electrical power system (EPS), the communication system (COM) for telemetry; the star tracker (ST) and the attitude and orbit control system (AOCS) performing attitude determination and attitude control. Each of these systems is embedded on a different PCB as shown in the avionics stack module of Figure 5.

3.2. Attitude Determination and Control System (ADCS)

The attitude determination and control system (ADCS) performs an important role in the mission objectives of the satellite. The main components of the ADCS are embedded in the OBC within the avionics stack (see Figure 5). The ADCS

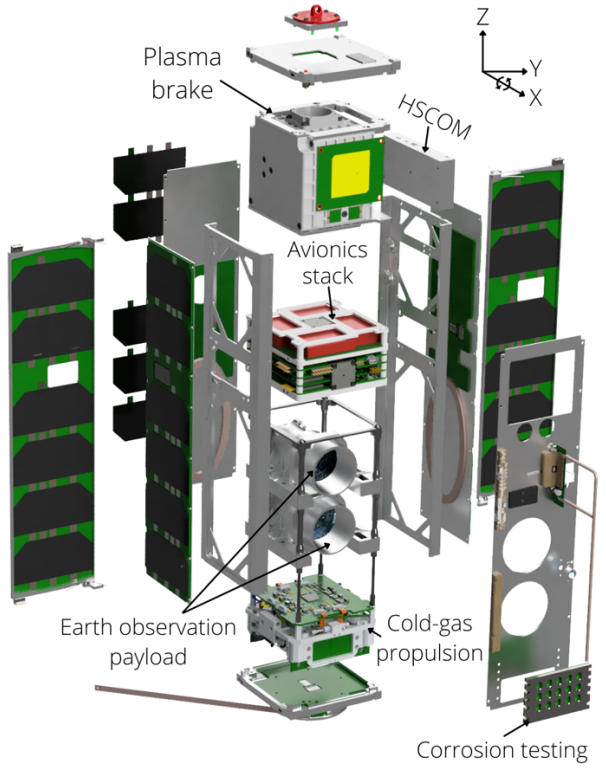

Figure 4. Exploded view of ESTCube-2 3U CubeSat [1].

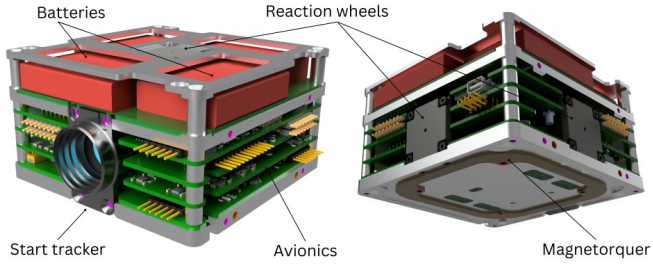

Figure 5. ESTCube-2 satellite avionics stack module [1].

subsytem can be sub divided into three major blocks which work together in fulfilling mission requirements. These blocks are: sensors, actuators and algorithms embedded in the OBC as seen in Figure 6.

Based on the mission requirements, a star tracker (ST) system and a cold gas propulsion system are introduced to enable the ADCS functionality beyond the Earth's magnetic field. This concept stems from the interest in developing further deep space mission (ESTCube-LuNa mission). However, these systems still serve as a necessary backup option on the ESTCube-2 design. The sensors on the ESTCube-2 satellite comprises the following:

- Magnetometers
- Gyroscopes
- Accelerometers
- Sun sensors
- Star tracker

On the OBC board are two redundant sets of MEMS sensors: two magnetometers (LIS3MDL), two gyroscopes (BMG160) and an accelerometer (FXOS8700CQ) in each set. There is an additional magnetometer on each of the side panels of

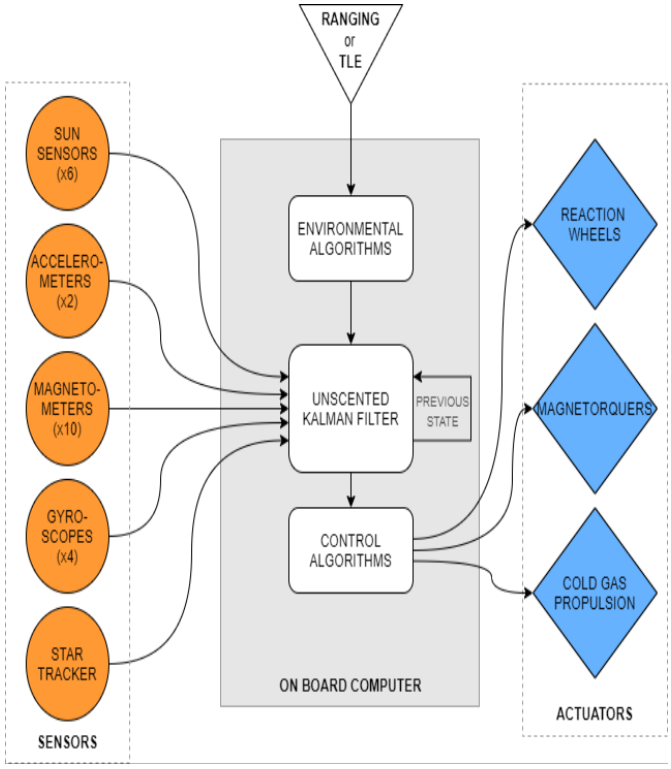

Figure 6. ESTCube-2 ADCS [2].

Figure 7. ESTCube-2 Magnetorquers [1].

ESTCube-2 for a better characterisation of the residual magnetic field of the satellite. There is a two-axis sun sensor located at the middle of every side of the satellite. the sun sensors which are developed in-house are based on an evolved design similar to the ESTCube-1.

As indicated in Figure 6, the actuators onboard the satellite are:

- Three coreless magetorquers with a magnetic moment of 0.45 Am^2, designed in-house as shown in Figure 7;
- Three Hyperion Technologies RW210 Series nanosatellite RWs. Measuring 25 $mm \times 25\ mm \times 15\ mm^3$, mass: 32 g and momentum storage: 3.0 $mNms$;
- Three Wittenstein Cyber Motors CYBER2 nanosatellite RWs for redundancy. Measuring: 20 $mm \times 20\ mm \times 20\ mm$, Mass: 30 g, Momentum storage: 2.0 $mNms$;
- GOMSpace NanoProp CGP3 cold gas propulsion (CGP) system.

The ADCS makes use of Unscented Kalman Filter (UKF) to interpret sensory data and account for uncertainties that arise from various sensory measurements. While the UKF provides the most probable attitude of the satellite, the control

algorithms aim to calculate the required control values for various actuators on board the satellite. The ESTCube-2's mission requirement provides for certain maneuvers to be executed, employing the use of sensors and actuators availble for deep-space missions.

Based on mission requirements, the ADCS is expected to execute four main control maneuvers:

- Detumbling to establish reliable communication between the satellite and ground segments mainly achieved by the B-dot control algorithm;
- Satellite pointing for Earth Observation camera operations as well as high-speed data downlink;
- Reaction wheel unloading/desaturating for continuous operations; and
- Satellite spin-up for experiment deployment.

The popular B-dot algorithm making use of magnetorquers is utilized for the detumbling operations, while a specialized regulator is used for the cold gas propulsion system which will be tested for deep-space operations. The spin-up of the satellite for the PB technology demonstration is also done by CGP and magnetorquers as backup.

For satellite pointing maneuvers, the RW is used with various control laws as previously discussed and simulated in [8], [10]. The satellite can also makes use of magnetorquers in a PD-like control law for pointing operations. Similar control laws are also employed for unloading and desaturating of the RWs, while further tests for unloading of the RW using the CGP are required for the deep-space operations. Based on the pointing maneuver, FTC schemes are designed in this thesis [11].

4. FAULT TOLERANT CONTROL DESIGNS FOR ESTCUBE-2

Generally, the design of the attitude control system for satellites necessitates a robust actuation system that offers precise control. Depending on the size and mass of satellites, the available actuators used to obtain such precise control typically have some limitations in their capacity. If the capacity is exceeded, a specific actuator might fail to provide the required precise control, leading to actuator saturation. This could compromise system performance and induce instability. Due to fault and/or failure on a particular actuator, saturation may occur on other actuators as a result of over reliance and excessive generation of torque in the case of a RW. Actuator faults and saturation are considered collectively in Chapter 4.2.

4.1. Mathematical Modelling

According to the governing laws of dynamics, applying a force to a body anywhere other than its center of mass will induce a rotational intent in the body. The relationship between the body's rotation and its momentum is defined as

$$h = J\omega \tag{4.1}$$

where h is the body's momentum, J is the inertia matrix and ω is the angular velocity.

4.1.1. Inertia Matrix

The inertia matrix J can be obtained by relating the location of a portion of mass from the center of a body, r , and its angular velocity as shown in Equation 4.2

$$h = \int r \times (\omega \times r) dm \tag{4.2}$$

The inertia matrix J about an arbitrary origin is then given below based on cross products of individual elements:

$$J = \begin{bmatrix} J_x & -J_{xy} & -J_{xz} \\ -J_{yx} & J_y & -J_{yz} \\ -J_{zx} & -J_{zy} & J_z \end{bmatrix} \tag{4.3}$$

$$J = \begin{bmatrix} \int_v (y^2+z^2)\rho_m dv & -\int_v (xy)\rho_m dv & -\int_v (xz)\rho_m dv \\ -\int_v (yx)\rho_m dv & \int_v (x^2+z^2)\rho_m dv & -\int_v (yz)\rho_m dv \\ -\int_v (xz)\rho_m dv & -\int_v (zy)\rho_m dv & \int_v (x^2+y^2)\rho_m dv \end{bmatrix} \tag{4.4}$$

where

- ρ_m is the density of the satellite
- v is represented as the volume

and J_x, J_y and J_z are the moments of inertia about the x, y and z axis respectively, and $J_{xy} = J_{yx}$, $J_{xz} = J_{zx}$ and $J_{yz} = J_{zy}$ are the products of inertia.

If the principal axes of inertia coincide with the axes of the body frame by being symmetric with its axes $J_{xy} = J_{xz} = J_{yz} = 0$, the inertia matrix reduces to:

$$J = \begin{bmatrix} J_x & 0 & 0 \\ 0 & J_y & 0 \\ 0 & 0 & J_z \end{bmatrix} \tag{4.5}$$

4.1.2. Dynamics

Based on the Quaternion model earlier discussed and its advantages in space technology applications over the Euler angle representations, the spacecraft dynamics model here is derived, reviewed and simplified in terms of quaternions. The satellite is assumed to be a rigid body and a point mass in orbit to derive the dynamic model. Therefore with Newton-Euler formulation and application of Newton's second law to the spacecraft rotational motion;

$$M = \dot{h}_i \tag{4.6}$$

where

- h is the angular momentum
- M is the applied torque or external moment in inertial frame with reference to body frame

in view of Coriolis Equation [47], Equation 4.6 can be expressed as

$$M = \dot{h} + \omega_i \times h \tag{4.7}$$

and the rate of angular momentum can be defined as

$$\dot{h} = J\dot{\omega}_i = -\omega_i \times J\omega_i + M \tag{4.8}$$

M can be expressed as addition of all disturbance torques and a control torque T_c

$$J\dot{\omega}_i = T_d + T_c - \omega_i^{\times} J\omega_i. \tag{4.9}$$

where

T_d is the sum of disturbance torques acting on the satellite;
T_c is the applied control input torque;
$\omega \in \mathbb{R}^3$ is the angular velocity vector of the spacecraft;
$J\dot{\omega}_i$ is the rate of angular momentum $\dot{h}$ in the inertial reference frame;

$\omega_i^{\times}$ is the skew symmetric representation of the angular velocity in the inertial reference frame.

$$\omega_i^{\times} = \begin{bmatrix} 0 & -\omega_3 & \omega_2 \\ \omega_3 & 0 & -\omega_1 \\ -\omega_2 & \omega_1 & 0 \end{bmatrix} \tag{4.10}$$

The satellite model with RW can be described with respect to Nadir direction as

$$J\dot{\omega}_i = T_d + T_c - \omega_i^{\times}(J\omega_i + H) \tag{4.11}$$

where the angular momentum of the wheel $H = [h_1\ h_2\ h_3]^T$ is added to obtain the effective angular momentum of the satellite in the inertial reference frame. The satellite's angular velocity can also be represented by body frame rotation relative to the orbit frame as described in [10].

4.1.3. Kinematics

The kinematic model tends to describe the orientation of the satellite with integration of the angular velocity. The kinematic model expressed in quaternions are derived based on [48].

$$\dot{q_v} = -\frac{1}{2}\omega \times\ q_v + \frac{1}{2}q_0\omega \tag{4.12}$$

$$\dot{q_0} = -\frac{1}{2}\omega^T q_v \tag{4.13}$$

The reduced kinematic equation is given by

$$\begin{bmatrix} \dot{q_1} \\ \dot{q_2} \\ \dot{q_3} \end{bmatrix} = \frac{1}{2}\begin{bmatrix} q_0 & -q_3 & q_2 \\ q_3 & q_0 & -q_1 \\ -q_2 & q_1 & q_0 \end{bmatrix}\begin{bmatrix} \omega_1 \\ \omega_2 \\ \omega_3 \end{bmatrix} \tag{4.14}$$

where $[q_1, q_2, q_3]$ are vector components of q_v.

4.1.4. Linearization

Inorder to evenutally proceed with controller design, a linearization of the nonlinear plant model is required. To do this, a linearization about an attitude equilibrium point of $q_0 = 1$ and $q_1, q_2, q_3 = 0$ based on first-order Taylor series expansion [49, Sec. 3.2.2] is achieved. Equation 4.15 represents the partial derivative as a function g of q and ω_i of the kinematic equation given in Equation 4.14

$$\dot{q_v} = \frac{\partial g}{\partial q}(q) + \frac{\partial g}{\partial \omega_i}(\omega_i) \tag{4.15}$$

with the consideration of $\omega_i = 0$ at equilibrium point,

$$\dot{q} - \dot{q_{eq}} = \frac{\partial g}{\partial q}(q - q_{eq}) + \frac{\partial g}{\partial \omega_i}(\omega_i - \omega_{ieq}) \tag{4.16}$$

Therefore Equation 4.14 can further be expanded as

$$\begin{bmatrix} \dot{q_1} \\ \dot{q_2} \\ \dot{q_3} \end{bmatrix} = \begin{bmatrix} 0 & 0 & 0 & \frac{1}{2}(q_0) & 0 & 0 \\ 0 & 0 & 0 & 0 & \frac{1}{2}(q_0) & 0 \\ 0 & 0 & 0 & 0 & 0 & \frac{1}{2}(q_0) \end{bmatrix} \begin{bmatrix} q_1 \\ q_2 \\ q_3 \\ \omega_1 \\ \omega_2 \\ \omega_3 \end{bmatrix} \tag{4.17}$$

Based on state space model $\dot{x} = Ax + Bu$ with $u = T_c$, and approximation of Equation 4.9 ($J\dot{\omega}_i \approx T_c$) with negligible disturbance torque and $q_0 = 1$ at equilibrium:

$$A = \begin{bmatrix} 0_3 & \frac{1}{2}(I_3) \\ 0_3 & 0_3 \end{bmatrix}, x = \begin{bmatrix} q_v \\ \omega_i \end{bmatrix}, B = \begin{bmatrix} 0_3 \\ J^{-1} \end{bmatrix} \tag{4.18}$$

The linearized model of ESTCube-2 $G(s)$ in state space form with neglected angular momentum of RW based on approximation and simplicity used in obtaining the AW compensator $K_{AW}(s)$ is given as

$$\begin{bmatrix} \dot{q_v} \\ \dot{\omega_i} \end{bmatrix} = \begin{bmatrix} 0 & 0 & 0 & 0.5 & 0 & 0 \\ 0 & 0 & 0 & 0 & 0.5 & 0 \\ 0 & 0 & 0 & 0 & 0 & 0.5 \\ f_{41} & 0 & 0 & 0 & 0 & f_{46} \\ 0 & f_{52} & 0 & 0 & 0 & 0 \\ 0 & 0 & f_{63} & f_{64} & 0 & 0 \end{bmatrix} \begin{bmatrix} q_v \\ \omega_i \end{bmatrix} + \begin{bmatrix} 0 & 0 & 0 \\ 0 & 0 & 0 \\ 0 & 0 & 0 \\ 1 & 0 & 0 \\ 0 & 1 & 0 \\ 0 & 0 & 1 \end{bmatrix} (T_c) \tag{4.19}$$

with functions $f_{41}, f_{46}, f_{52}, f_{63}, f_{64}$ given below and $\omega_o = 2\pi/T_o$.

$$\begin{aligned} f_{41} &= 8(J_z - J_y)\omega_o^2 - 2\omega_o \\ f_{46} &= (-J_x - J_z + J_y)\omega_o \\ f_{52} &= 6(J_z - J_x)\omega_o^2 \\ f_{63} &= 2(J_x - -J_y)\omega_o^2 - 2\omega_o \\ f_{64} &= -f_{46} \end{aligned} \tag{4.20}$$

4.2. Actuator Fault/Failure and Saturation Modelling

This thesis focuses on addressing actuator faults and saturation, particularly concerning the collective behaviour of the RWs, given their susceptibility to torque/momentum

capacity limitations. Specifically, RW saturation occurs when these components cannot deliver the necessary and excess torque beyond their designated specifications.

The RW considered in the ESTCube-2 case has a momentum storage of about 1.5×10^{-3} *Nms*. The RW has a spinning wheel and an electric motor. The motor produces a required torque based on conservation of angular momentum controlled by an embedded computer. As the RW is not a linear system, the torque produced is not directly proportional to the current applied. The nonlinearity in the RW is mostly as a result of friction [50], which tends to delay the rotation of the motor until the stator current threshold is attained. By application of a rotating mass with inertia J_{rw} and damping coefficient b, the RW can be modeled as shown in Equation 4.21.

$$\dot{h} = J_{rw}\dot{\omega} + b\omega \tag{4.21}$$

where $\dot{h}$ is the rate of angular momentum or the applied wheel torque.

To further consider the full model of the system with addition of the fault/failure and saturation modelling, the faults are classified mainly into four categories based on their effects on the RW. These are:

- F1: Decreased reaction torque,
- F2: Increased bias torque,
- F3: Failure to respond to control signals,
- F4: Continuous generation of reaction torque.

Since RWs are considered to be sensitive and vulnerable to sources of faults as described in [51], the faults are described based on loss of actuator effectiveness fault (F1), bias fault (F2), outage failure (F3) and hard-over failure (F4) respectively. The faults itemized F1–F4 can be mathematically modeled as

$$T_{ci} = e_i(t)\tau_{di} + \bar{\tau}_i \tag{4.22}$$

where
T_{ci} as indicated in Equation 4.9 is the actual control torque input on the spacecraft;
τ_{di} is the desired torque signal for each n reaction wheels;
$e_i(t)$ indicates the effectiveness value of the i^{th} reaction wheel between 0 and 1; and
$\bar{\tau}_i$ is the uncertain input fault on the satellite.

A summary of the reaction wheel faults and the model parameters is shown in Table 1. The hard-over failure is a result of continuous increase or decrease in the speed of the wheel, which in turn generates a continuous torque irrespective of the control input signal. In the case of no fault, the actual control torque from the reaction wheel is equal to the desired torque signal with $T_{ci} = \tau_{di}$, where $e_i(t) = 1$ and $\bar{\tau}_i = 0$.

Table 1. Reaction Wheel Faults and Parameters

Fault	**Type**	$\bar{\tau}_i$	e_i
F1	Loss of actuator effectiveness	0	$0 < e_i < 1$
F2	Bias	$\bar{\tau}_i \neq 0$	1
F3	Outage	0	0
F4	Hard-over	$\bar{\tau}_i \neq 0$	0

Equation 4.23 gives the actual control input torque T_c by n reaction wheels.

$$T_c = E(t)\tau_d + \bar{\tau} \tag{4.23}$$

where
$\tau_d = [\tau_{d1}\ \tau_{d2}\ ....\ \tau_{dn}]^T \in \mathbb{R}^n$ is the commanded torque vector from the n actuators;
$E(t) = diag[e_1(t), e_2(t), ..., e_n(t)] \in \mathbb{R}^{n\times n}$ indicates the actuator effectiveness matrix; and
$\bar{\tau} = [\bar{\tau}_1\ \bar{\tau}_2\ ....\ \bar{\tau}_n]^T \in \mathbb{R}^n$ is the uncertain fault vector based on additive torque from F2 and F4.

The combined satellite model from Equation 4.11 , with addition of actuator fault is given in Equation 4.24 with the accompanying assumptions:

$$J\dot{\omega}_i = T_d + E(t)\tau_d + \bar{\tau} - \omega_i^{\times}(J\omega_i + H). \tag{4.24}$$

Assumption 1: The additive torque from F2 and F4 may be uncertain; however, there exists a positive scalar quantity f_0 that bounds it such that $||\bar{\tau}|| \leq f_0$.

Assumption 2: The external disturbance torque represented by T_d is also uncertain but bounded by a positive scalar quantity.

In the event of actuator failure, the remaining actuators need to exert more torque than optimal to compensate for the failed actuator and maintain system stability. However, this increased effort can lead to actuator saturation, potentially causing system instability. Actuator saturation can involve both magnitude and rate limitations. This thesis specifically focuses on magnitude saturation, as it affects the angular momentum of the wheel. When addressing magnitude saturation in the Reaction Wheel (RW), the thesis introduces a non-linear constraint with bounded saturation limits defined as $|h_i| \leq h_{max}$.

4.3. Anti-Windup Compensator Design

As described briefly in Chapter 2.4, the approach to the AW design is as given in [18] [46]. The approach relies mostly on guaranteeing stability for various plant structures ($G(s) \in \mathscr{RH}_\infty$) with input saturation and gives the assurance that there exists an AW compensator which can globally stabilize the system provided the AW compensator is of the same order as the plant, referred to as a Full-Order AW

Compensator. This section will give a brief review of the full-order AW design based on description in [18].

4.3.1. MIMO Full-Order AW Design

A typical AW configuration is shown in Figure 8 with the plant $G(s)$ assumed to be stable ($G(s) \in \mathscr{RH}_\infty^{p\times m}$). In this configuration, $K(s)$ is the nominal controller, $u \in \mathbb{R}^m$ is the unsaturated control signal, $u_m \in \mathbb{R}^m$ is the saturated control signal (plant input), $r \in \mathbb{R}^n$ is the reference, $y \in \mathbb{R}^p$ is the plant output and $\Theta(s)$ is the anti-windup compensator. The state space satellite system $G(s) \in \mathscr{RH}_\infty^{p\times m}$ is given as

$$G(s) \sim \left[\begin{array}{c|c} A_p & B_p \\ \hline C_p & D_p \end{array}\right] \tag{4.25}$$

with $A_p \in \mathbb{R}^{n\times n}$, and B_p, C_p, D_p as known real matrices with appropriate dimensions. The control plant input $u_m = sat(u)$ is based on the saturation function defined in Section 2.4. The full-order AW compensator provides stability and improvements based on techniques of [18, 46, 52] and has the following structure

$$K_\Theta(s) = \begin{bmatrix} M(s) - I \\ G(s)M(s) \end{bmatrix} \tag{4.26}$$

where $M(s) \in \mathscr{RH}_\infty^{m\times m}$ is the chosen right factor stable transfer function matrix of a right coprime factorisation of the plant $G(s) = N(s)M^{-1}(s)$. The coprime factorization has to be of the same order as the plant so that the AW compensator can have the formulation

$$K_\Theta(s) = \begin{bmatrix} M(s) - I \\ N(s) \end{bmatrix} \sim \left[\begin{array}{c|c} A_p + B_pF & B_p \\ \hline F & 0 \\ \hline C_p + D_pF & D_p \end{array}\right]. \tag{4.27}$$

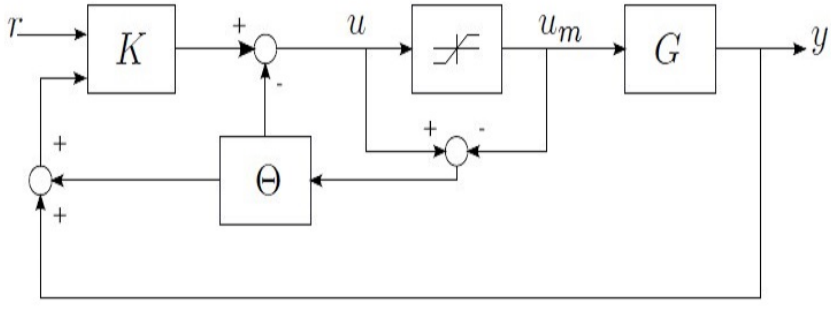

Figure 8. Typical Anti-Windup Configuration

where F is chosen so that $A_p + B_p F$ is Hurwitz[1] and $N(s) = G(s)M(s)$ is the disturbance filter. Based on the above AW compensator structure, an equivalent representation is shown in Figure 9 in which the structure is decoupled into a nominal linear system, a nonlinear loop and a disturbance filter ($N(s)$). In this representation, the nominal linear system only determines the overall system behaviour if no saturation occurs ($\tilde{u} = 0$). However if saturation occurs ($\tilde{u} \neq 0$) then the nonlinear loop and disturbance filter sections contribute in the system behaviour. Given that the nominal linear system from the above representation is designed to stabilise the plant $G(s)$ when no saturation occurs, the general stability of the entire system can then be a solution of finding if the nonlinear loop is stable. The deadzone operator used in the nonlinear loop is related to the saturation function as $D_z(u) = u - sat(u)$.

If the controller $K(s)$ has been designed to achieve a desired level of performance in nominal conditions, then we consider the system in Figure 9 as stable and y_d representing the deviation of the real output y from the nominal linear output y_{lin} which is affected by the control signal u_{lin}. This is further expressed by the mapping $\mathscr{T}_p : u_{lin} \mapsto y_d$ whereby the size of the mapping can be minimized by minimizing the $\mathscr{L}_2$ gain. With the state space realisation given in Equation 4.27, the AW problem becomes a solution of determining the matrix F which minimizes the $\mathscr{L}_2$ gain of the operator $\mathscr{T}_p$ while also guaranteeing asymptotic stability. Concepts from Lyapunov stability, $\mathscr{L}_2$ gain minimization and Circle criterion are used in achieving this [53–55]. Based on the evaluation of the inequality examined in [18], the system will be exponentially stable provided an $\mathscr{L}_2$ gain $\gamma > 0$. Results on the solution can further be found in the cited reference and are presented in the following theorem.

[1] where F is chosen so that $A_p + B_p F$ is Hurwitz

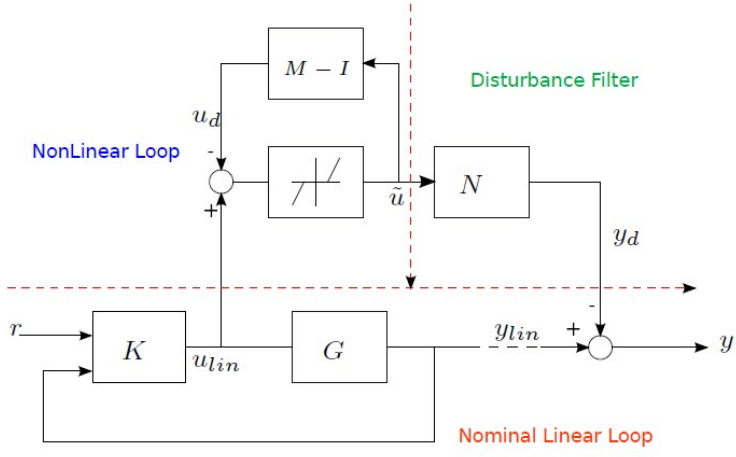

Figure 9. Equivalent Representation of AW Structure

Theorem 1 (4.3.1): Assume that $G \in \mathscr{RH}_\infty^{p\times m}$ and that the unconstrained relationship between $K(s)$ and $G(s)$ is stable. The system given is well-posed if there exist matrices $Q > 0$ and L and scalars $U > 0$ and $\gamma > 0$ such that the following linear matrix inequality holds[2]:

$$\text{He}\left\{\begin{bmatrix} A_pQ + B_pL & B_pU & 0 & 0 \\ -L & -2U & I & 0 \\ 0 & 0 & -\gamma & 0 \\ C_pQ + D_pL & D_pU & 0 & -\gamma \end{bmatrix}\right\} < 0 \tag{4.28}$$

If such matrices exist, then an AW compensator shown in Figure 9 ensuring global asymptotic stability can be constructed with Equation (4.27) by simply using $F = LQ^{-1}$ such that $||\mathscr{T}_p||_{\mathscr{L}_2} < \gamma$. If a measure of $\mathscr{L}_2$ gain obtained from Theorem 1 is not required, the following corollary may be used to construct the AW compensator instead.

Corollary 1: Assume the same conditions with K and G as in Theorem 1 are satisfied. Then the system in Figure 9 is globally asymptotically stable, well-posed and there exists a constant $\gamma > 0$ such that $||\mathscr{T}_p||_{\mathscr{L}_2} < \gamma$ if there exist matrices $Q > 0$ and L and a scalar $U > 0$ for the following linear matrix inequality to hold:

$$\begin{bmatrix} QA_p^T + A_pQ + B_pL + L^TB_p^T & B_pU - L^T \\ \star & -2U \end{bmatrix} < 0 \tag{4.29}$$

The proof of the above LMI is the same as was given in [18] for Theorem 1.

Remark 1: With choosing the transfer function matrix $M(s) \in \mathscr{RH}_\infty^{m\times m}$ as a factor of the coprime factorization of the plant, an AW compensator can be designed which may result in a system with higher order extra states and considered to be expensive computationally. In order to achieve reduced states or no extra states, a low order and static AW compensator can be introduced but $M(s)$ in this case is not chosen as the plant's coprime factorization but as a combination of the nominal controller and plant.

Remark 2: In a case where $G(s) \notin \mathscr{RH}_\infty$ the LMIs (4.28) and also Equation 4.29 become infeasible. In order to overcome this, a small change to the LMIs can be made such that: if there exist matrices $Q > 0$, diagonal $U > 0$ and L such that a new LMI can be obtained as in [18] then $F = LQ^{-1}$ can be used to contruct the AW compensator.

4.3.2. SISO/SIMO Full-Order AW Design

In the case of the SISO/SIMO system, the system has only one control input with one or possibly more than one output. In similar comparison with the MIMO case in previous section, consider the single loop AW compensator structure in Figure

[2] the notation $\text{He}\{A\} = A + A'$.

10 with its equivalent representation in Figure 11 with $G_i(s) \in \mathscr{RH}_\infty^{p_i \times 1}$ as the plant and state space realisation given as

$$G_i(s) \sim \left[\begin{array}{c|c} A_i & B_i \\ \hline C_i & D_i \end{array}\right] \tag{4.30}$$

where $A_i \in \mathbb{R}^{n_i \times n_i}$, $K_i(s)$ is the controller and $\Theta_i(s)$ is the AW compensator whose state space similar to Equation 4.27 is given as

$$K_{\Theta_i}(s) = \begin{bmatrix} M_i(s) - I \\ N_i(s) \end{bmatrix} \sim \left[\begin{array}{c|c} A_i + B_i F_i & B_i \\ \hline F_i & 0 \\ \hline C_i + D_i F_i & D_i \end{array}\right]. \tag{4.31}$$

Similar to previous section, all signals and parameters including u, $u_m \in \mathbb{R}$, $r \in \mathbb{R}$ and $y \in \mathbb{R}^{p_i}$ are as defined. Also, the mapping of $\mathscr{T}_p : u_{lin} \mapsto y_d$ is important to the AW performance and shows the deviation of the saturated state from the nominal linear state of the system. Additionally, similar to Theorem 1 (4.3.1), the following theorem satisfies the full order AW compensator design for the SISO/SIMO case.

Theorem 2 (4.3.2): Assume that $G_i \in \mathscr{RH}_\infty^{p_i \times 1}$ and that the nominal interconnection of $K_i(s)$ and $G_i(s)$ is asymptotically stable and well-posed. If there exist matrices $Q_i > 0$ and L_i and scalars $U_i > 0$ and $\gamma_i > 0$ such that the following linear matrix inequality holds:

$$\text{He}\left\{\begin{bmatrix} A_i Q_i + B_i L_i & B_i U_i & 0 & 0 \\ -L_i & -2U_i & I & 0 \\ 0 & 0 & -\gamma_i & 0 \\ C_i Q_i + D_i L_i & D_i U_i & 0 & -\gamma_i \end{bmatrix}\right\} < 0 \tag{4.32}$$

then the equivalent system in Figure 11 with AW compensator in Equation 4.31 where $F_i = L_i Q_i^{-1}$, globally exponentially stable, well-posed such that $||\mathscr{T}_p||_{\mathscr{L}_2} < \gamma$. Also, if the $\mathscr{L}_2$ gain obtained from the Theorem is not required (stability is the only concern), the following corollary may be used.

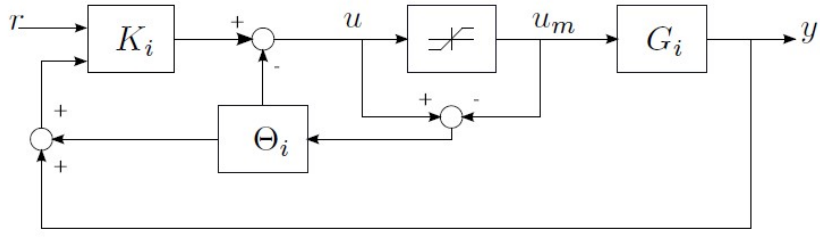

Figure 10. Single-loop AW Structure

Corollary 1: Assume that $G_i \in \mathscr{RH}_\infty^{p_i \times 1}$ and that the nominal interconnection of $K_i(s)$ and $G_i(s)$ is stable and well-posed. If there exist matrices $Q_i > 0$ and L_i and scalar $U_i > 0$ such that the following linear matrix inequality holds:

$$\begin{bmatrix} Q_i A_p^T + A_i Q_i + B_i L_i + L_i^T B_i^T & B_i U_i - L_i^T \\ \star & -2U_i \end{bmatrix} < 0 \tag{4.33}$$

then the equivalent system in Figure 11 with AW compensator in Equation 4.31 where $F_i = L_i Q_i^{-1}$, is globally exponentially stable, well-posed and there exist a $\gamma_i > 0$ such that $||\mathscr{T}_p||_{\mathscr{L}_2} < \gamma_i$.

Theorems 4.3.1 and 4.3.2 are presented in a manner that doesn't confine the plant and controller to a specific structure. They can be generalized and applied to any stabilizing plant and controller system. A more straightforward result and formulation, as presented, will be applied to the nanosatellite (ESTCube-2) model on the design of an appropriate AW compensator.

4.4. Integrated Anti-Windup FTC Design

In the design of the AW-FTC for the nanosatellite model, the non-linear plant model has to be linearized based on Equation 4.19. Also, the state space model ($\dot{x} = Ax + Bu$) represented in Equation 4.18 is used to create the system of LMIs and obtain variable matrices Q and L in Equations 4.28 and 4.29 to construct the AW compensator in Equation 4.27. The actual control outputs of the nanosatellite are the attitude in quaternion and the angular velocity of the nanosatellite. The control input (u) is the control torque (T_c) on the satellite.

The nominal controller ($K(s)$) has a PD controller structure with angular velocity and quaternion error q_e (given in Equation 2.24) as inputs. A decoupled

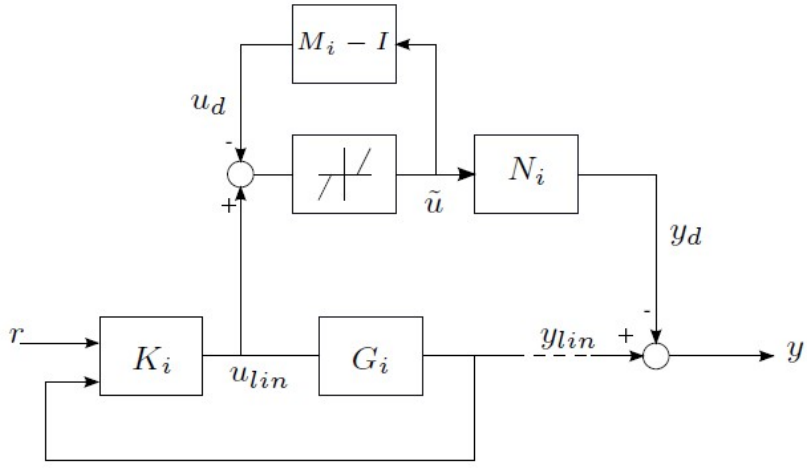

Figure 11. Equivalent Representation of Single-loop AW Structure

representation as shown in Figure 12 can be considered to have a plant structure as $G(s) = G_D(s)X$ as well as the controller such that $K(s) = X^{-1}K_D(s)$ where $K_D(s)$ is the nominal PD controller for each element of the state.

Given

$$G(s) = G_D(s)X, \quad K(s) = X^{-1}K_D(s) \tag{4.34}$$

where $X \in \mathbb{R}^{m\times m}$ is a static nonsingular matrix with its inverse considered as a control allocation matrix X^{-1}, $G_D(s)$ and $K_D(s)$ can be diagonal matrices as:

$$G_D(s) = blockdiag(G_1(s), G_2(s), ..., G_m(s)) \tag{4.35}$$

$$K_D(s) = blockdiag(K_1(s), K_2(s), ..., K_m(s)) \tag{4.36}$$

The quaternion error q_e with the desired quaternion q_d as well as the desired control torque are given below:

$$\begin{bmatrix} q_e \end{bmatrix} = \begin{bmatrix} q_{d0} & q_{d1} & -q_{d2} & -q_{d3} \\ -q_{d1} & q_{d0} & q_{d3} & -q_{d2} \\ q_{d2} & -q_{d3} & q_{d0} & -q_{d1} \\ q_{d3} & q_{d2} & q_{d1} & q_{d0} \end{bmatrix} \begin{bmatrix} q_0 \\ q_1 \\ q_2 \\ q_3 \end{bmatrix} \tag{4.37}$$

$$u_d = [u_{d1}\ u_{d2}\ u_{d3}]^T = \begin{bmatrix} k_\omega \omega_1 + k_q q_{e1} \\ k_\omega \omega_2 + k_q q_{e2} \\ k_\omega \omega_3 + k_q q_{e3} \end{bmatrix} \tag{4.38}$$

The following assumptions can be made about the plant and controller structure

Assumptions:

1. The plant and controller have the structure given in Eq 4.34.
2. The closed loop interconnection of the plant $G(s)$ and the controller $K(s)$ is asymptotically stable.

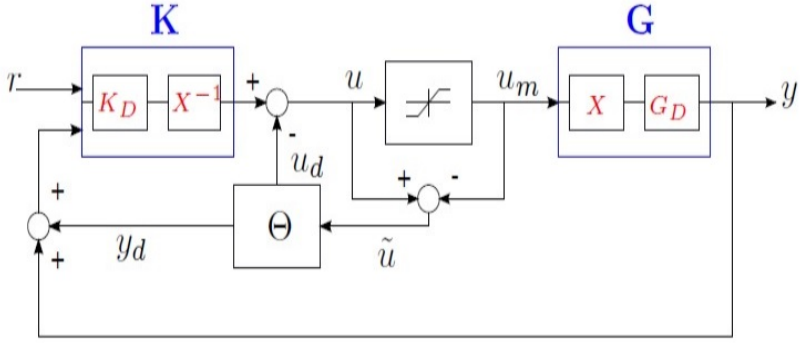

Figure 12. Full Anti-Windup Structure

3. $G(s) \in \mathscr{RH}_\infty$ (and by extension, each $G_i(s)$ for $i \in \{1,...,m\}$ is stable, i.e., $G_i(s) \in \mathscr{RH}_\infty$.

Based on the nominal control law presented in Equation 4.38, results of the simulation without an induced fault or saturation in the momentum storage of the wheels is presented in Figure 13. The result shows the attitude in quaternion stabilizes to Nadir pointing mode in about 4000 s and the angular velocity attenuates to 0 deg in about 750 s in all axes. The angular momentum of the wheel is also seen to accommodate the torque needed within the limit of the momentum storage, such that the performance is regulated for effective pointing manoeuvre.

The integrated AW–FTC is simulated based on satellite model with actuator faults discussed earlier in Equation 4.24. The faults are summed up with a generated effective torque based on the model. With the nominal controller under the induced faults, the system is unable to attain attitude stabilization with overloading of the wheels and saturation of the angular momentum. The initial angular velocity of the satellite is $(1,1,60)$ deg/s, while the saturation limits based on the reaction wheel momentum is placed at $\pm 1.5 \times 10^{-3} Nms$. Attitude stabilization is achieved in all three axes within about 1300 s as shown in Figure 14(a). Similarly, the angular velocity completely attenuates in about 1300 s as shown in Figure 14(b). The RW angular momentum varies intermittently within the limits, while the control input to the AW compensator is capped when no further torque is required (required torque becomes zero).

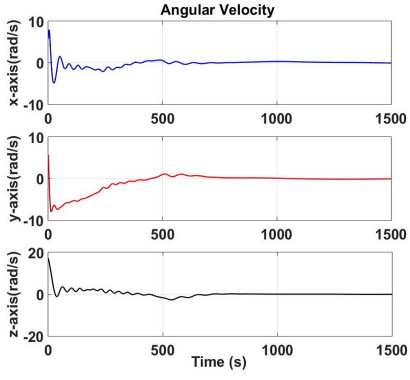

(a)

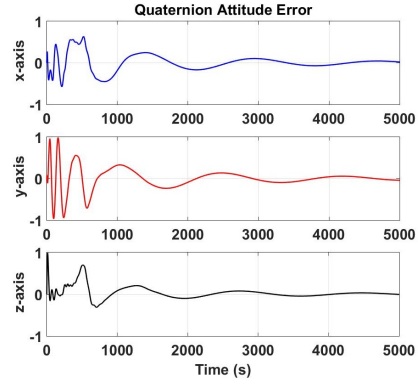

(b)

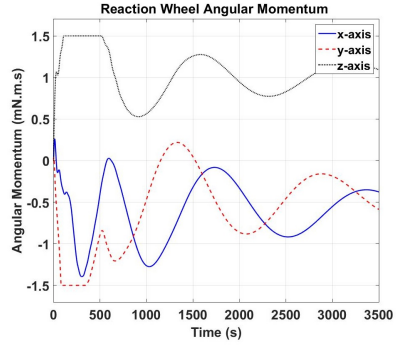

(c)

Figure 13. Nominal control law simulation result.

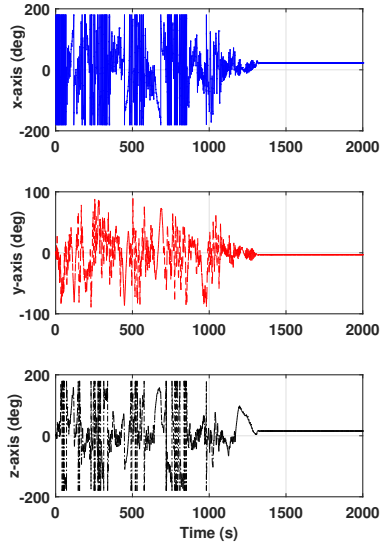

(a) Attitude Error

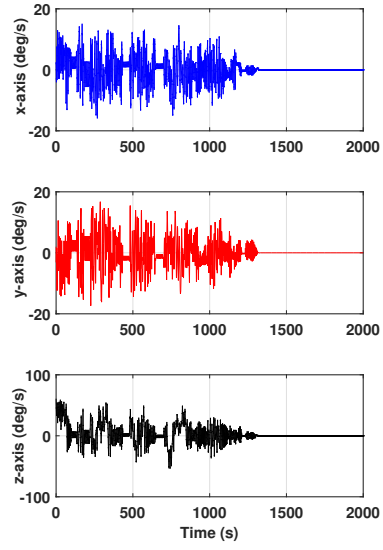

(b) Angular Velocity response

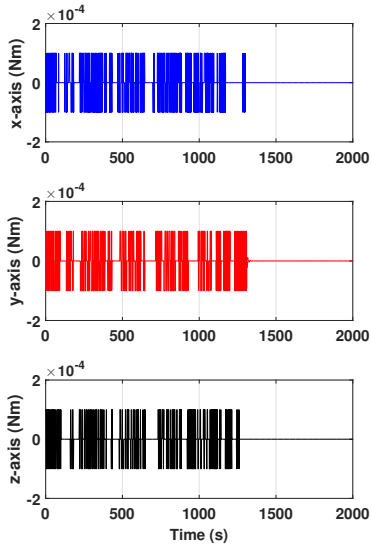

(c) RW torque response

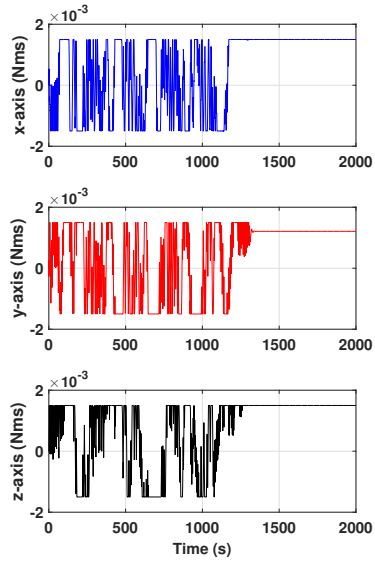

(d) RW angular momentum response

Figure 14. Control performance of Integrated AW–FTC architecture with RW fault and saturation.

5. INVESTIGATIONS OF MACHINE LEARNING ALGORITHMS ON FAULT TOLERANT CONTROL

Given the necessity for precise dynamic models, especially in scenarios involving failures, disturbances, gravitational models, and other uncertain nonlinear factors, it becomes crucial to employ robust approaches with adaptive schemes. This adaptability is essential to accommodate the inherent complexity of space missions.

Reinforcement Learning (RL) which has become increasingly important in several fields and applications can be used to address aforementioned issues and failures typical of space missions. RL is a sub division of ML with supervised and unsupervised learning as other approaches. While supervised learning aims to learn by exploiting and comparing input-output data pairs as inputs and targets, unsupervised learning aims to extrapolate certain patterns and properties/features of the dataset, typically expressing a probability distribution of the dataset. Table 2 gives a summary of the learning approaches.

Table 2. Summary of Different Learning Approaches

Learning Approach	**Remarks**	**Task Type**	**Algorithms/Methods**
Supervised Learning	This system tends to learn by exploiting input-output dataset pairs	Classification	Artificial Neural Networks, Nearest Neighbour, Discriminant Analysis, Support Vector Machines
		Regression	Artificial Neural Networks, Linear Regression, Decision Trees, Ensemble methods, Support Vector Machines
Unsupervised Learning	This system tends to learn by considering the structure of the dataset and extrapolating patterns and features	Clustering	Artificial Neural Networks, Hidden Markov Models, Guassian Mixture, K-means, Hierarchical Clustering
		Dimensionality Reduction	Artificial Neural Networks, Principal Component Analysis, Linear Discriminant Analysis
Reinforcement Learning	This system tends to learn the action to take inorder to maximize reward based on certain inputs	Model-based	Model-established methods, Model-learned methods
		Model-free	Value iteration methods, Policy-iteration methods

5.1. Reinforcement Learning

Reinforcement learning (RL), unlike supervised and unsupervised learning is a kind of learning that relies on the environment to obtain a feedback into the network from the environment as opposed to learning from a dataset provided based

on a supervisor. RL is basically learning what to do, how to do (mapping) in-order to maximize numerical reward. The learner is not directed on action to take, rather explores which actions would yield the most reward [3]. The categories of RL involves states (x_t), actions (a_t) and rewards (r_t). The actions taken could also affect the environment, so the RL can be modelled as a Markov Decision Process (MDP) with state space (X), action space (A) and reward function as $r(x_t, a_t)$.

RL typically involves three concepts; a policy (π), a reward function (r_t) and a value function.

- Policy: A policy refers to a mapping from a perceived state of the environment to actions to be taken in those states.
- Reward Function: The reward function defines the goal in terms of numeric value (reward) sent by the environment to the agent indicating the desirability of that state.
- Value Function: Similar to the reward function but returns the total amount of reward an agent can accumulate from that state to the future.

The reinforcement learning theory suggests that an agent can obtain a policy which provides the mapping between states $x \in \mathbb{X}$ where $\mathbb{X}$ is a set of possible states, for an action $a \in \mathbb{A}$, where $\mathbb{A}$ is a set of possible actions. Using a transition probability $p(x_{t+1}|x_t, a_t)$, the dynamics of the agent can be represented from one state to another at a given time interval. The policy can follow a conditional probability distribution across the states which can either be deterministic $\pi(x_t)$ or stochastic $\pi(a_t|x_t)$. A reward $r(x_t, a_t)$ is received each time the agent performs an action and then aims to maximize the accumulated discount reward given by the function in Equation 5.2 from a given time t to a future time T.

$$\mathbb{R} = \sum_{i=t}^{T} \gamma^{i-t} r(x_i, a_i) \tag{5.1}$$

Where the coefficient γ is the discount factor between 0 and 1, which expresses the preference of rewards at a given time to future rewards. Recall, the value function V^{π} is the total amount of reward an agent can accumulate from that state to the future. Therefore the value function with a policy is given below:

$$V^{\pi}(x_t) = \mathbb{E}[\mathbb{R}|x_t, a_t = \pi(x_t)] \tag{5.2}$$

While RL methods are either model-based or model-free, the latter is usually considered common where the agent learns an optimal policy by interacting with the environment without knowledge of the state transition probability distribution and reward function [3, 56]. Figure 15 shows the interaction between the agent and environment based on the MDP [3]. RL approaches can be classified into two main categories:

- Value iteration method: Aims to find good estimate for the value function by iteratively updating the estimate to obtain an optimal state value function.

- Policy iteration method: Involves choosing a policy π and then iteratively evaluate the policy based on the state value function and improve it.

Spacecraft control problems have been considered with the policy iteration learning method [3, 57], where a parameterized policy is learnt such that:

$$\pi_\theta := \pi(a|s,\theta) \tag{5.3}$$

where $\theta \in \mathbb{R}^d$ is the parameter vector for the policy. The policy aims to find the probability that an action a is taken when the environment is in a state s. While the value function method relies on the value function, the policy iterative approach selects actions without input from the value function, whereby the value function may be used to learn the policy parameter θ.

A variant of the Proximal Policy Optimization (PPO) algorithm which is a policy iteration-based method for a discrete control scenario to address problem of orienting a spacecraft to a reference attitude by means of torque values which are discretized is considered by Elkins et al. [58]. In this work, the attitude controller (agent) performs large angle slews and stabilizes the system about the desired orientation maintaining the pointing accuracy requirement. Similarly, the authors in Vedant et al. [4] proposed an RL method based on the PPO algorithm for the ACS. The rigid body of the spacecraft is represented with the environment model, while the state space is defined by the error quaternion vector. Figure 16 shows the reinforcement learning method for the attitude control problem with the PPO. In this method, a curriculum learning based method is used to support the RL training whereby the agent is first trained with an initial state environment close to the target state and then a difficulty parameter is linearly introduced and increased to strengthen the problem. This method shows slightly better performance than the classical quaternion rate feedback (QRF) control.

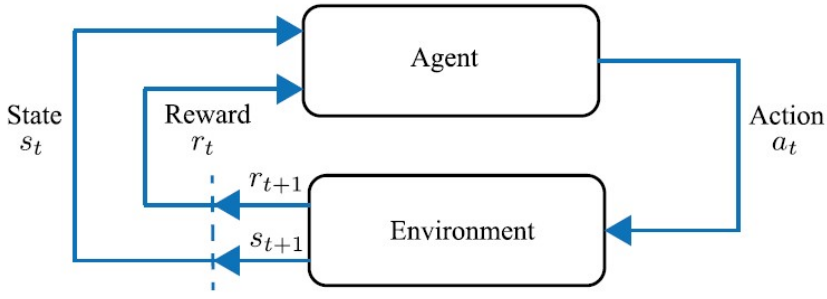

Figure 15. The interaction between Agent and Environment from Sutton et al. [3]

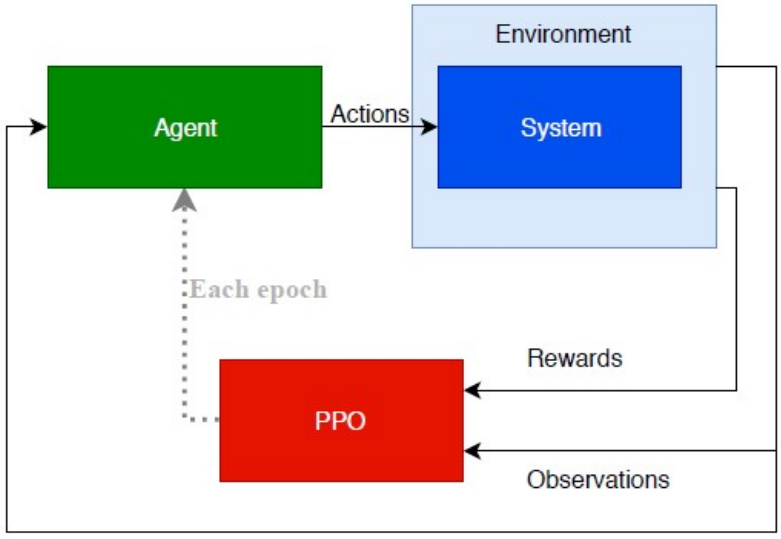

Figure 16. RL design with PPO from Vedant et al. [4]

Some other RL approaches have been studied and shown to produce better performance in comparison with PID controllers based on rise time and susceptibility to noise [59–61]. The stabilization of satellite attitude is considered in [59] and [61], while in [60], an orientation tracking problem is addressed in which the ACS consists of two neural networks (NN) for both angular rate control and orientation control. The angular rate controller is first implemented to guarantee an angular rate below a certain threshold in which the orientation controller activates once the spacecraft angular rate drops to achieve the desired attitude angles.

The attitude angle and angular velocity limits are considered as state constraints in the design of a practical ACS in Dong et al. [62]. In the design, a novel RL algorithm is introduced to account for the state constraints by introduction of barrier functions to encode the information of the forbidden region of the attitude and angular velocity limits into the cost function. Additionally, both real time and past data are used in updating the NN weights during the learning process. The study shows a reduced computational complexity in updating the NN weights in comparison with model predictive control methods.

5.2. Adaptive Neuro-Fuzzy Inference System Design

Amongst recent and advanced intelligent control approaches is the Adaptive Neuro-Fuzzy Inference System (ANFIS) which has provided promising results with control strategies aimed at adapting to constantly changing conditions (environment). The ANFIS can be seen as an approach of artificial intelligence that combines the

benefits of both neural networks and fuzzy logic systems [5]. The system aims to learn and make decisions based on analysed data just like other neural network approaches, but also has the ability to process incomplete data like a fuzzy logic system.

In this section, the ANFIS controller is implemented to explore its performance on the design of spacecraft control with nominal PID control and the Anti-windup compensator already designed. The ANFIS controller aims at reducing computational complexity and settling time while also encouraging the effective performance of actuator in the presence of uncertainty and disturbances. In the ANFIS design, the fuzzy inference system is applied to a feed forward adaptive neural network architecture that consist of 5 layers. The layers each contains a number of adaptive nodes with parameters described by a first order Takagi-Sugeno (TS) fuzzy model [63], with two fuzzy if-then rules each defining a linear relationship between the inputs and outputs.

$$Rule1 : If\ x\ is\ A_1\ and\ y\ is\ B_1\ then\ f_1 = p_1x + q_1y + r_1 \tag{5.4}$$

$$Rule2 : If\ x\ is\ A_2\ and\ y\ is\ B_2\ then\ f_2 = p_2x + q_2y + r_2 \tag{5.5}$$

The functions of each layer and node depicted in Figure 17 is described as follows:

Layer 1: The node output in this layer is defined by the membership function of input variables.

$$O_{1,i} = m_{A_i}(x)\ for\ i = 1,2$$

$$O_{1,i} = m_{B_{i-2}}(y)\ for\ i = 3,4$$

Layer 2: Product of membership function for each input variables called *firing strength*

$$O_{2,i} = \omega_i = m_{A_i}(x) \times m_{B_i}(y)\ for\ i = 1,2$$

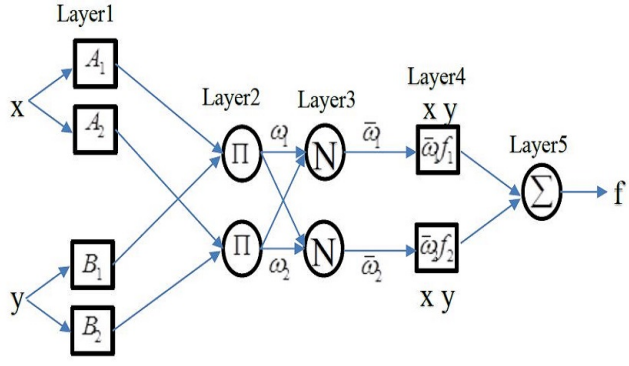

Figure 17. Architecture of Adaptive Neuro-Fuzzy Inference System [5]

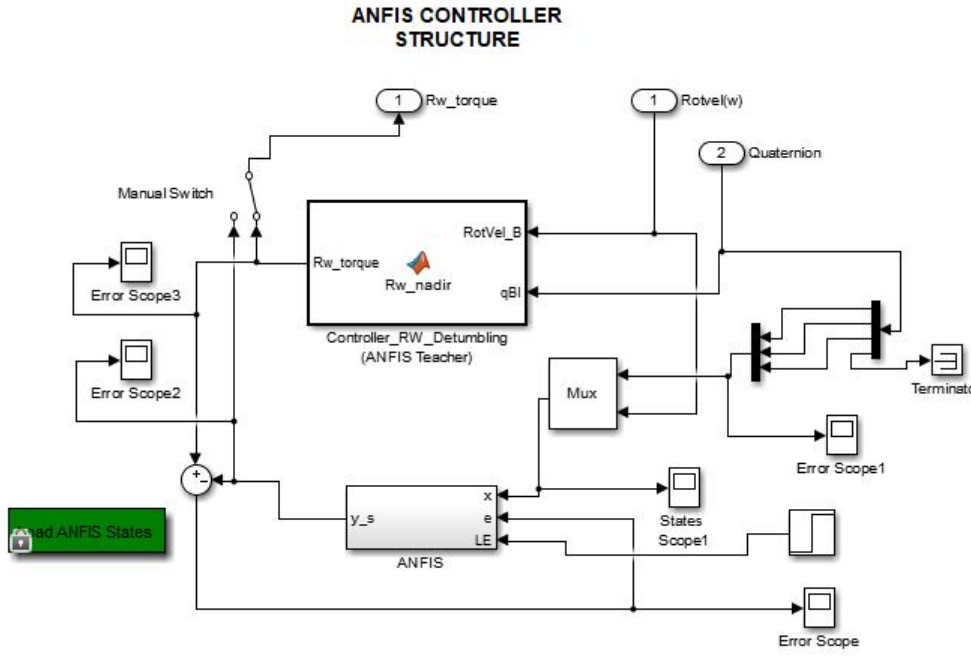

Figure 18. ANFIS controller simulation block structure

Layer 3: Normalize output of layer 2 called *normalized firing strength*

$$O_{3,i} = \bar{\omega}_i = \omega_i/(\omega_1 + \omega_2) \; for \; i = 1,2$$

Layer 4: Each node is an adaptive node with a node function which is a linear combination of input variables based on first order TS model.

$$O_{4,i} = \bar{\omega}_i f_i = \bar{\omega}_i(p_i x + q_i y + r_i)$$

where p_i, q_i, r_i are called *consequent parameters*.

Layer 5: This single node output is the summation of all incoming nodes from previous layers.

$$O_{5,i} = \sum_i \bar{\omega}_i f_i = \sum_i \omega_i f_i / \sum_i \omega_i$$

The input variables to the controller block in Figure 18 are angular velocities ω_i and quaternion attitude q_e errors similar to the integrated anti-windup architecture previously described. The output variable is the control torque generated as T_c (u_d). The ANFIS controller performs the unsupervised learning and takes in angular velocity and quaternion attitude error states as input. An initial training of the model is done to record initial states to be used in further iterations.

To verify the performance of the designed ANFIS controller, Table 3 lists parameters and details of the control implementation in simulation. The satellite's moment-of-inertia matrix is given as $diag[0.033\ 0.033\ 0.0067]\ kg.m^2$. Figure 19 presents simulation result of the ANFIS controller attaining stability even with induced fault. Compared to the nominal response presented in Figure 13, the ANFIS controller aims to stabilize the satellite attitude and attenuate the angular velocity within a set time, while ensuring that the initial saturation of the angular momentum does not affect the desired control scheme. The result is of interest and reveals promising performance as it has reduced computational complexity for the entire complex system. The settling time can also be improved with optimization on the ANFIS model's learning rate.

Parameter	**Value**
Satellite mass	$4\ kg$
RW maximum torque	$1 \times 10^{-4}\ Nm$
RW maximum angular momentum	$1.5 \times 10^{-3}\ Nms$
Initial angular velocity	$(0,0,12)\ deg/s$
AW γ^2	1.8124
K_q	0.01
K_ω	0.002

Table 3. Simulation Parameters

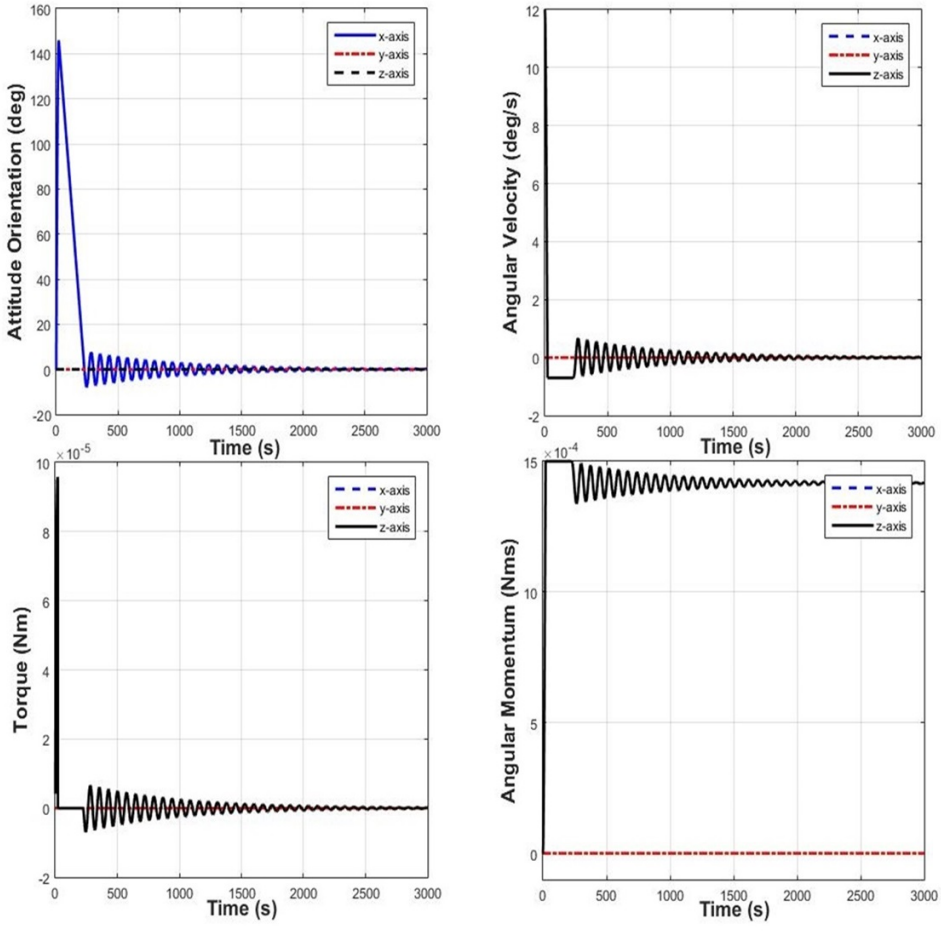

Figure 19. ANFIS controller response based on induced fault and saturation

6. CONCLUSION AND FUTURE WORK

This thesis presents the fault tolerant control architecture designed for ESTCube-2 nanosatellite. The main focus is to present a fault tolerant attitude control architecture able to tackle and handle concerns of faults/failure and saturation of actuators on nanosatellites considering the ESTCube-2 model. Recall the mission objective of the ESTCube-2 to demonstrate the plasma brake technology based on electric solar wind sail in Low Earth Orbit (LEO). In achieving this, the tether on board the plasma brake module is charged in synchronization with the controlled satellite spin rate. Together with other mission objectives, specific requirements for the Attitude Determination and Control System (ADCS) of ESTCube-2 were identified, including spin-up manoeuvres, angular momentum provision, spin control for tether deployment, and precise pointing accuracy and stability of 0.25 deg and 0.125 deg/s respectively. As the results of the PhD thesis rely on simulations, the implementation in orbit is currently delayed due to the unforeseen ESTCube-2 deployment failure from the launch vehicle. Further investigation is under-way to gather accurate information and provide an updated overview of the situation and the current status of ESTCube-2 at the time of this thesis submission.

The research aim of the thesis is therefore to develop a Fault-Tolerant Control (FTC) architecture tailored for the ESTCube-2 nanosatellite, with a specific focus on mitigating faults, failures, and disturbances without the need for explicit fault identification, thereby addressing the imperative of reducing computational complexity. In contrast to the ADCS design of the ESTCube-1 mission, this thesis focuses on the FTC design that also guarantees finite time stabilization. The proposed integrated anti-windup (AW) fault-tolerant control architecture, encompassing both full-order Multiple-Input, Multiple-Output (MIMO) AW compensators and Single-Input, Single-Output (SISO)/Single-Input, Multiple-Output (SIMO) designs, targets the dynamic structure of the ESTCube-2 nanosatellite.

Of notable significance is the introduction of the channel-by-channel AW compensator approach (SISO/SIMO), wherein individual compensators are designed for each control channel of the nanosatellite. This approach, characterized by its transparency and flexibility, enables independent design and alteration of each channel, demonstrating commendable performance. The full-order AW compensator, simulated based on set requirements with satellite dynamics, also proves effective, with both designs showcasing the capability to handle actuator magnitude saturation. Importantly, the research findings indicate that the performance of the AW compensator extends beyond satellite structures, suggesting broader applicability to systems modeled as a series interconnection of dynamic parts. This versatility positions the proposed fault-tolerant control architecture as a valuable contribution not only to satellite engineering but also to a wider spectrum of dynamic systems.

The thesis also proposes a combined architecture with the adaptive neuro-fuzzy inference system (ANFIS) controller, aimed at exploring the resourcefulness of neural network and fuzzy logic system. The result shows that the ANFIS controller provided a smoother control reaction on the actuators even with induced faults. Further investigations are recommended to validate dynamic states under various conditions, reflecting data from an observer. While the entire architecture addresses faults and uncertainties, future work suggests exploring larger-scale, varying faults, uncertainties, and disturbances. Model-free approaches, particularly utilizing algorithms such as Proximal Policy Optimization (PPO), are proposed for enhanced effectiveness in handling these scenarios. The overarching implication is that the developed fault-tolerant control methods and architectures, initially tailored for space applications, hold potential for broader implementation across diverse systems, contributing to advancements in modern control engineering.

SUMMARY

This research is carried out at the University of Tartu, Tartu Observatory, the Finnish Meteorological Institute and the Estonian Student Satellite Programme. This thesis presents the ESTCube-2 attitude determination and control system (ADCS). ESTCube-2 is a satellite built according to the three-unit CubeSat standard. The main scientific mission of ESTCube-2 is to perform the in-orbit electric solar wind sail demonstration. The electric solar wind sail is a propellant-less propulsion technology concept. Ultimately, the ESTCube-2 nanosatellite will aim to demonstrate technologies for deep interplanetary space mission of CubeSats and nanosatellites.

This thesis focuses on designing a fault-tolerant control architecture for the ESTCube-2 nanosatellite, which is tasked with demonstrating plasma brake technology in Low Earth Orbit (LEO). The satellite has specific requirements for its ADCS to achieve its mission objectives, including tether deployment and angular momentum control with pointing accuracy and pointing stability of $0.25\,\mathrm{deg}$ and $0.125\,\mathrm{deg}/s$ respectively. The research aims to provide a fault-tolerant control (FTC) architecture that can handle faults and disturbances without the need to identify the faults, thus reducing computational complexity. An integrated anti-windup fault-tolerant control architecture is proposed. This includes the design of an anti-windup (AW) compensator, which addresses actuator saturation. Two design approaches are discussed: a full-order multi-input multi-output (MIMO) AW compensator and single-input/single-output (SISO) or single-input/multi-output (SIMO) designs. The SISO/SIMO approach is considered for each individual control channel, providing transparency and flexibility for independent channel design and tuning.

The AW compensator's performance is found to be promising, reducing computational burden and simplifying channel tuning. The thesis also proposes a combination of this architecture with an Adaptive Neuro-Fuzzy Inference System (ANFIS) controller, which offers smoother control reactions in the presence of faults.

SISUKOKKUVÕTE

Veakindel asendikontrollisüsteem nanosatelliitidele ESTCube-2 näitel

Käesolev uurimus viidi läbi Tartu Ülikoolis, Tartu Observatooriumis, Soome meteoroloogiainstituudis ja Eesti Tudengisatelliidi programmis. See töö käsitleb ESTCube-2 asendi määramise ja kontrolli süsteemi (ADCS). ESTCube-2 on kolmeühikuline kuupsatelliit. ESTCube-2 missiooni peamine teaduslik eesmärk on katsetada orbiidil elektrilist päikesepurje. Elektriline päikesepuri on kütusevaba tõukesüsteemi kontseptsioon. ESTCube-2 proovib demonstreerida uusi tehnoloogiad, mis võimaldaks planeerida süvakosmose missioone kuup- ja nanosatelliitidele. See töö keskendub veakindla kontrollsüsteemi arendamisele ESTCube-2 satelliidi jaoks, mille eesmärgiks on testida plasmapidurit maa-lähedasel orbiidil (LEO).

Missiooni õnnestumiseks on asendi määramise ja kontrolli süsteemil kindlad nõuded, mille hulgas on lõõa välja laskmine ja pöördemomendi täpsuse ja stabiilsuse kontroll vastavalt 0.25 kraadi ja 0.125 kraadi/s täpsusega. Antud uurimuse eesmärk on luua veakindel süsteem (FTC), mis käsitleb vigu ja ebakorrapärasusi ilma vajaduseta neid tuvastada, vähendades süsteemi arvutuslikku keerukust. Selleks on välja pakutud integreeritud anti-windup (AW) tõrkekindel juhtsüsteem. See süsteem hõlmab anti-windup kompensaatori disaini, mis käsitleb täiturite küllastumist. Käsitletakse kahte lahendust: mitme-sisendi/mitme-väljundiga (MIMO) ja ühe-sisendi/ühe-väljundiga (SISO) või ühe-sisendi/mitme-väljundiga (SIMO) AW kompensaatorit. Iga üksiku kontrollkanali puhul kaalutakse SISO/SIMO lähenemisviisi, mis tagab läbipaistvuse ja paindlikkuse sõltumatu kanali kavandamisel ja häälestamisel. AW-kompensaatori jõudlus on paljutõotav, vähendades arvutuskoormust ja lihtsustades kanali häälestamist. Töös pakutakse välja ka selle arhitektuuri kombinatsioon adaptiivse Neuro-Fuzzy Inference System (ANFIS) kontrolleriga, mis pakub sujuvamaid kontrollreaktsioone rikete korral.

BIBLIOGRAPHY

[1] J. Dalbins, K. Allaje, H. Ehrpais, I. Iakubivskyi, E. Ilbis, P. Janhunen, J. Kivastik, M. Merisalu, M. Noorma, M. Pajusalu *et al.*, "Interplanetary student nanospacecraft: Development of the leo demonstrator estcube-2," *Aerospace*, vol. 10, no. 6, p. 503, 2023.

[2] I. Ofodile, H. Teras, A. Slavinskis, and G. Anbarjafari, "Towards an integrated fault tolerant control for estcube-2 attitude control system," in *2022 IEEE Aerospace Conference (AERO)*. IEEE, 2022, pp. 1–11.

[3] R. S. Sutton and A. G. Barto, *Reinforcement learning: An introduction*. MIT press, 2018.

[4] J. T. Vedant, "Reinforcement learning for spacecraft attitude control," in *70th International Astronautical Congress*, 2019.

[5] J.-S. Jang, "Anfis: adaptive-network-based fuzzy inference system," *IEEE transactions on systems, man, and cybernetics*, vol. 23, no. 3, pp. 665–685, 1993.

[6] A. Slavinskis, M. Pajusalu, H. Kuuste, E. Ilbis, T. Eenmäe, I. Sünter, K. Laizans, H. Ehrpais, P. Liias, E. Kulu *et al.*, "ESTCube-1 in-orbit experience and lessons learned," *IEEE Aerospace and Electronic Systems Magazine*, vol. 30, no. 8, pp. 12–22, 2015.

[7] H. Ehrpais, J. Kütt, I. Sünter, E. Kulu, A. Slavinskis, and M. Noorma, "Nanosatellite spin-up using magnetic actuators: Estcube-1 flight results," *Acta Astronautica*, vol. 128, pp. 210–216, 2016.

[8] I. Ofodile, J. Kütt, J. Kivastik, M. K. Nigol, A. Parelo, E. Ilbis, H. Ehrpais, and A. Slavinskis, "Estcube-2 attitude determination and control: Step towards interplanetary cubesats," in *2019 IEEE Aerospace Conference*. IEEE, 2019, pp. 1–12.

[9] A. Slavinskis, U. Kvell, E. Kulu, I. Sünter, H. Kuuste, S. Lätt, K. Voormansik, and M. Noorma, "High spin rate magnetic controller for nanosatellites," *Acta Astronautica*, vol. 95, pp. 218–226, 2014.

[10] I. Ofodile, H. Ehrpais, A. Slavinskis, and G. Anbarjafari, "Stabilised LQR control and optimised spin rate control for nanosatellites," in *2019 9th International Conference on Recent Advances in Space Technologies (RAST)*. IEEE, 2019, pp. 715–722.

[11] I. Ofodile, N. Ofodile-Keku, P. Jemitola, G. Anbarjafari, and A. Slavinskis, "Integrated anti-windup fault-tolerant control architecture for optimized satellite attitude stabilization," *IEEE Journal on Miniaturization for Air and Space Systems*, vol. 2, no. 4, pp. 189–198, 2021.

[12] I. Ofodile, A. Adebomehin, P. Jemitola, A. Slavinskis, and G. Anbarjafari, "Nanosatellite attitude stabilization based on decentralized anti-windup fault

tolerant control," in *2023 IEEE Aerospace Conference*. IEEE, 2023, pp. 1–7.

[13] S. Cao and Y. Zhao, "Anti-disturbance fault-tolerant attitude control for satellites subject to multiple disturbances and actuator saturation," *Nonlinear Dynamics*, vol. 89, no. 4, pp. 2657–2667, 2017.

[14] J. Boada, C. Prieur, S. Tarbouriech, C. Pittet, and C. Charbonnel, "Anti-windup design for satellites control with microthrusters," in *AIAA Guidance, Navigation, and Control Conference*, 2009, p. 5950.

[15] ——, "Extended model recovery anti-windup for satellite control," *IFAC Proceedings Volumes*, vol. 43, no. 15, pp. 205–210, 2010.

[16] S. Lätt, A. Slavinskis, E. Ilbis, U. Kvell, K. Voormansik, E. Kulu, M. Pajusalu, H. Kuuste, I. Stinter, T. Eenmaee *et al.*, "Estcube-1 nanosatellite for electric solar wind sail in-orbit technology demonstration," *Proceedings of the Estonian Academy of Sciences*, vol. 63, no. 2, pp. 200–209, 2014.

[17] I. Iakubivskyi, P. Janhunen, J. Praks, V. Allik, K. Bussov, B. Clayhills, J. Dalbins, T. Eenmäe, H. Ehrpais, J. Envall *et al.*, "Coulomb drag propulsion experiments of ESTCube-2 and FORESAIL-1," *Acta Astronautica*, vol. 177, pp. 771 – 783, 2020.

[18] M. C. Turner, G. Herrmann, and I. Postlethwaite, "Incorporating robustness requirements into antiwindup design," *IEEE Transactions on Automatic Control*, vol. 52, no. 10, pp. 1842–1855, 2007.

[19] B. Wie, H. Weiss, and A. Arapostathis, "Quarternion feedback regulator for spacecraft eigenaxis rotations," *Journal of Guidance, Control, and Dynamics*, vol. 12, no. 3, pp. 375–380, 1989.

[20] J. Jiang, "Fault-tolerant control systems-an introductory overview," *Acta Automatica Sinica*, vol. 31, no. 1, pp. 161–174, 2005.

[21] M. Mariton, "Detection delays, false alarm rates and the reconfiguration of control systems," *International Journal of Control*, vol. 49, no. 3, pp. 981–992, 1989.

[22] R. Kristiansen, P. J. Nicklasson, and J. T. Gravdahl, "Satellite attitude control by quaternion-based backstepping," *IEEE transactions on control systems technology*, vol. 17, no. 1, pp. 227–232, 2009.

[23] Y. Zhang and J. Jiang, "Bibliographical review on reconfigurable fault-tolerant control systems," *Annual reviews in control*, vol. 32, no. 2, pp. 229–252, 2008.

[24] M. Benosman, "A survey of some recent results on nonlinear fault tolerant control," *Mathematical Problems in Engineering*, vol. 2010, pp. 1–25, January 2010.

[25] H. Alwi and C. Edwards, "Fault tolerant control using sliding modes with

on-line control allocation," in *Fault tolerant flight control*. Heidelberg, Germany: Springer, 2010, pp. 247–272.

[26] Q. Hu, "Robust adaptive sliding-mode fault-tolerant control with l2-gain performance for flexible spacecraft using redundant reaction wheels," *IET control theory & applications*, vol. 4, no. 6, pp. 1055–1070, 2010.

[27] A. de Ruiter, "A fault-tolerant magnetic spin stabilizing controller for the jc2sat-ff mission," *Acta Astronautica*, vol. 68, no. 1, pp. 160–171, 2011.

[28] S. Shi, B. Yuan, K. Zhao, Z. You, and G. Zhang, "Fault-tolerant attitude determination and control system design of nanosatellite 2," *Journal of Aerospace Engineering*, vol. 31, no. 6, p. 04018087, 2018.

[29] Godard and K. D. Kumar, "Fault tolerant reconfigurable satellite formations using adaptive variable structure techniques," *Journal of guidance, control, and dynamics*, vol. 33, no. 3, pp. 969–984, 2010.

[30] Q. Shen, D. Wang, S. Zhu, and K. Poh, "Finite-time fault-tolerant attitude stabilization for spacecraft with actuator saturation," *IEEE Transactions on Aerospace and Electronic Systems*, vol. 51, no. 3, pp. 2390–2405, 2015.

[31] F. Liming, H. HUANG, and Z. Kaixing, "Robust fault-tolerant attitude control for satellite with multiple uncertainties and actuator faults," *Chinese Journal of Aeronautics*, 2020.

[32] S. M. Amrr, A. Banerjee, and M. Nabi, "Fault-tolerant attitude control of small spacecraft using robust artificial time-delay approach," *IEEE Journal on Miniaturization for Air and Space Systems*, vol. 1, no. 3, pp. 179–187, 2020.

[33] Q. Hu, X. Huo, and B. Xiao, "Reaction wheel fault tolerant control for spacecraft attitude stabilization with finite-time convergence," *International Journal of Robust and Nonlinear Control*, vol. 23, no. 15, pp. 1737–1752, 2013.

[34] H. Lee and Y. Kim, "Fault-tolerant control scheme for satellite attitude control system," *IET control theory & applications*, vol. 4, no. 8, pp. 1436–1450, 2010.

[35] L. Zaccarian and A. R. Teel, *Modern anti-windup synthesis: control augmentation for actuator saturation*. Princeton University Press, 2011, vol. 36.

[36] C. Yang, L. Zhang, and J. Sun, "Anti-windup controller design for singularly perturbed systems subject to actuator saturation," *IET Control Theory & Applications*, vol. 10, no. 4, pp. 469–476, 2016.

[37] N. A. Ofodile and M. C. Turner, "Anti-windup design for input-coupled double integrator systems with application to quadrotor uav's," *European Journal of Control*, vol. 38, pp. 22–31, 2017.

[38] S. Tarbouriech, G. Garcia, J. M. G. da Silva Jr, and I. Queinnec, *Stability and*

stabilization of linear systems with saturating actuators. Springer Science & Business Media, 2011.

[39] S. Galeani, S. Tarbouriech, M. Turner, and L. Zaccarian, "A tutorial on modern anti-windup design," *European Journal of Control*, vol. 15, no. 3-4, pp. 418–440, 2009.

[40] S. Tarbouriech and M. Turner, "Anti-windup design: an overview of some recent advances and open problems," *IET control theory & applications*, vol. 3, no. 1, pp. 1–19, 2009.

[41] G. Grimm, I. Postlethwaite, A. R. Teel, M. C. Turner, and L. Zaccarian, "Linear matrix inequalities for full and reduced order anti-windup synthesis," in *American Control Conference, 2001. Proceedings of the 2001*, vol. 5. IEEE, 2001, pp. 4134–4139.

[42] G. Grimm, A. R. Teel, and L. Zaccarian, "Linear lmi-based external anti-windup augmentation for stable linear systems," *Automatica*, vol. 40, no. 11, pp. 1987–1996, 2004.

[43] K. Groves, A. Serrani, S. Yurkovich, M. Bolender, and D. Doman, "Anti-windup control for an air-breathing hypersonic vehicle model," in *AIAA guidance, navigation, and control conference and exhibit*, 2006, p. 6557.

[44] C. Burgat and S. Tarbouriech, "Intelligent anti-windup for systems with input magnitude saturation," *International Journal of Robust and Nonlinear Control: IFAC-Affiliated Journal*, vol. 8, no. 12, pp. 1085–1100, 1998.

[45] A. R. Teel and N. Kapoor, "The l 2 anti-winup problem: Its definition and solution," in *1997 European Control Conference (ECC)*. IEEE, 1997, pp. 1897–1902.

[46] P. F. Weston and I. Postlethwaite, "Linear conditioning for systems containing saturating actuators," *Automatica*, vol. 36, no. 9, pp. 1347–1354, 2000.

[47] A. A. White and R. Bromley, "Dynamically consistent, quasi-hydrostatic equations for global models with a complete representation of the coriolis force," *Quarterly Journal of the Royal Meteorological Society*, vol. 121, no. 522, pp. 399–418, 1995.

[48] J. R. Wertz, *Spacecraft attitude determination and control*. Springer Science & Business Media, 2012, vol. 73.

[49] Y. Yang, "Spacecraft attitude determination and control: Quaternion based method," *Annual Reviews in Control*, vol. 36, no. 2, pp. 198–219, 2012.

[50] V. Carrara and H. K. Kuga, "Current and speed control operating modes of a reaction wheel," *Applied Mechanics and Materials*, vol. 706, pp. 170–180, 2015.

[51] S. Murugesan and P. Goel, "Fault-tolerant spacecraft attitude control system," *Sadhana*, vol. 11, no. 1-2, pp. 233–261, 1987.

[52] N. A. Ofodile and M. C. Turner, "Decentralized approaches to antiwindup design with application to quadrotor unmanned aerial vehicles," *IEEE Transactions on Control Systems Technology*, vol. 24, no. 6, pp. 1980–1992, 2016.

[53] H. K. Khalil, "Nonlinear systems, 3rd," *New Jewsey, Prentice Hall*, vol. 9, 2002.

[54] H. J. Marquez, *Nonlinear control systems: analysis and design*. John Wiley Hoboken, NJ, USA, 2003, vol. 161.

[55] M. Arcak and P. Kokotović, "Nonlinear observers: a circle criterion design and robustness analysis," *Automatica*, vol. 37, no. 12, pp. 1923–1930, 2001.

[56] D. P. Bertsekas, "Feature-based aggregation and deep reinforcement learning: A survey and some new implementations," *IEEE/CAA Journal of Automatica Sinica*, vol. 6, no. 1, pp. 1–31, 2018.

[57] D. Bertsekas, *Reinforcement learning and optimal control*. Athena Scientific, 2019.

[58] J. Elkins, R. Sood, and C. Rumpf, "Autonomous spacecraft attitude control using deep reinforcement learning," in *71st International Astronautical Congress (IAC)*, vol. 2020, 2020.

[59] R. Su, F. Wu, and J. Zhao, "Deep reinforcement learning method based on ddpg with simulated annealing for satellite attitude control system," in *2019 Chinese Automation Congress (CAC)*. IEEE, 2019, pp. 390–395.

[60] D. Yadava, R. Hosangadi, S. Krishna, P. Paliwal, and A. Jain, "Attitude control of a nanosatellite system using reinforcement learning and neural networks," in *2018 IEEE Aerospace Conference*. IEEE, 2018, pp. 1–8.

[61] D. Gao, H. Zhang, C. Li, and X. Gao, "Satellite attitude control with deep reinforcement learning," in *2020 Chinese Automation Congress (CAC)*. IEEE, 2020, pp. 4095–4101.

[62] H. Dong, X. Zhao, and H. Yang, "Reinforcement learning-based approximate optimal control for attitude reorientation under state constraints," *IEEE Transactions on Control Systems Technology*, vol. 29, no. 4, pp. 1664–1673, 2020.

[63] T. Takagi and M. Sugeno, "Fuzzy identification of systems and its applications to modeling and control," *IEEE transactions on systems, man, and cybernetics*, no. 1, pp. 116–132, 1985.

ACKNOWLEDGEMENTS

The support for this project was provided through the EU Regional Development Fund and the Estonian Research Council Grant (PUT638). I extend my gratitude to all those who contributed to this thesis. Special appreciation goes to my supervisors for their guidance and support during the research. I would like to acknowledge the ESTCube team and the iCV research group for their platform and support. I express thanks to Johan Kütt and Mihkel Pajusalu for their valuable support, and Mart Noorma for his thorough review. A heartfelt thank you to my family, partner, and siblings for their unwavering support and encouragement throughout this endeavor.

PUBLICATIONS

CURRICULUM VITAE

Personal data

Name:	Ikechukwu Ofodile
Birth:	31 August 1993
Citizenship:	Nigerian
Languages:	English
Phone:	+2347016626179
Email:	i.ofodile@ut.ee

Education

2018 –	PhD Engineering and Technology (Physical Information Technology) – University of Tartu, Estonia
2016 – 2017	MSc Robotics and Computer Engineering – University of Tartu, Estonia
2013 – 2016	BSc Electrical and Electronics Engineering – Eastern Mediterranean University Cyprus

Employment

2018 – 2022	Research Assistant, University of Tartu, Estonia
2017 –2018	Researcher and Instructor, Air Force Research and Development Centre. Nigerian Air Force
2016 – 2017	Graduate Research Assistant, Institute of Technology, University of Tartu

Scientific work

Main fields of interest:

- Fault Tolerant Control
- Attitude Control
- AI Semantic Segmentation

ELULOOKIRJELDUS

Isikuandmed

Nimi:	Ikechukwu Ofodile
Sünd:	31. august 1993
Kodakondsus:	Nigeeria
Keeled:	inglise
Telefon:	+2347016626179
E-post:	i.ofodile@ut.ee

Haridus

2018 –	PhD tehnika ja tehnoloogia (füüsiline infotehnoloogia) – Tartu Ülikool, Eesti
2016 – 2017	MSc robootika ja arvutitehnika – Tartu Ülikool, Eesti
2013 – 2016	BSc elektri- ja elektroonikatehnika – Ida-Vahemere Ülikool Küpros

Teenistuskäik

2018 – 2022	Teadusassistent, Tartu Ülikool, Eesti
2017 – 2018	õhuväe teadus- ja arenduskeskuse teadur ja instruktor. Nigerian Air Jõud
2016 – 2017	Tartu Ülikooli Tehnoloogiainstituudi kraadiõppe assistent

Teadustegevus

Peamised uurimisvaldkonnad:

- Veakindel juhtimine
- Suhtumise juhtimine
- AI semantiline segmenteerimine

DISSERTATIONES TECHNOLOGIAE UNIVERSITATIS TARTUENSIS

1. **Imre Mäger**. Characterization of cell-penetrating peptides: Assessment of cellular internalization kinetics, mechanisms and bioactivity. Tartu 2011, 132 p.
2. **Taavi Lehto**. Delivery of nucleic acids by cell-penetrating peptides: application in modulation of gene expression. Tartu 2011, 155 p.
3. **Hannes Luidalepp**. Studies on the antibiotic susceptibility of *Escherichia coli*. Tartu 2012, 111 p.
4. **Vahur Zadin**. Modelling the 3D-microbattery. Tartu 2012, 149 p.
5. **Janno Torop**. Carbide-derived carbon-based electromechanical actuators. Tartu 2012, 113 p.
6. **Julia Suhorutšenko**. Cell-penetrating peptides: cytotoxicity, immunogenicity and application for tumor targeting. Tartu 2012, 139 p.
7. **Viktoryia Shyp**. G nucleotide regulation of translational GTPases and the stringent response factor RelA. Tartu 2012, 105 p.
8. **Mardo Kõivomägi**. Studies on the substrate specificity and multisite phosphorylation mechanisms of cyclin-dependent kinase Cdk1 in *Saccharomyces cerevisiae*. Tartu, 2013, 157 p.
9. **Liis Karo-Astover**. Studies on the Semliki Forest virus replicase protein nsP1. Tartu, 2013, 113 p.
10. **Piret Arukuusk**. NickFects–novel cell-penetrating peptides. Design and uptake mechanism. Tartu, 2013, 124 p.
11. **Piret Villo**. Synthesis of acetogenin analogues. Asymmetric transfer hydrogenation coupled with dynamic kinetic resolution of α-amido-β-keto esters. Tartu, 2013, 151 p.
12. **Villu Kasari**. Bacterial toxin-antitoxin systems: transcriptional cross-activation and characterization of a novel *mqsRA* system. Tartu, 2013, 108 p.
13. **Margus Varjak**. Functional analysis of viral and host components of alphavirus replicase complexes. Tartu, 2013, 151 p.
14. **Liane Viru**. Development and analysis of novel alphavirus-based multifunctional gene therapy and expression systems. Tartu, 2013, 113 p.
15. **Kent Langel**. Cell-penetrating peptide mechanism studies: from peptides to cargo delivery. Tartu, 2014, 115 p.
16. **Rauno Temmer**. Electrochemistry and novel applications of chemically synthesized conductive polymer electrodes. Tartu, 2014, 206 p.
17. **Indrek Must**. Ionic and capacitive electroactive laminates with carbonaceous electrodes as sensors and energy harvesters. Tartu, 2014, 133 p.
18. **Veiko Voolaid**. Aquatic environment: primary reservoir, link, or sink of antibiotic resistance? Tartu, 2014, 79 p.
19. **Kristiina Laanemets**. The role of SLAC1 anion channel and its upstream regulators in stomatal opening and closure of *Arabidopsis thaliana.* Tartu, 2015, 115 p.

20. **Kalle Pärn**. Studies on inducible alphavirus-based antitumour strategy mediated by site-specific delivery with activatable cell-penetrating peptides. Tartu, 2015, 139 p.
21. **Anastasia Selyutina**. When biologist meets chemist: a search for HIV-1 inhibitors. Tartu, 2015, 172 p.
22. **Sirle Saul**. Towards understanding the neurovirulence of Semliki Forest virus. Tartu, 2015, 136 p.
23. **Marit Orav**. Study of the initial amplification of the human papillomavirus genome. Tartu, 2015, 132 p.
24. **Tormi Reinson**. Studies on the Genome Replication of Human Papillomaviruses. Tartu, 2016, 110 p.
25. **Mart Ustav Jr**. Molecular Studies of HPV-18 Genome Segregation and Stable Replication. Tartu, 2016, 152 p.
26. **Margit Mutso**. Different Approaches to Counteracting Hepatitis C Virus and Chikungunya Virus Infections. Tartu, 2016, 184 p.
27. **Jelizaveta Geimanen**. Study of the Papillomavirus Genome Replication and Segregation. Tartu, 2016, 168 p.
28. **Mart Toots**. Novel Means to Target Human Papillomavirus Infection. Tartu, 2016, 173 p.
29. **Kadi-Liis Veiman**. Development of cell-penetrating peptides for gene delivery: from transfection in cell cultures to induction of gene expression *in vivo*. Tartu, 2016, 136 p.
30. **Ly Pärnaste**. How, why, what and where: Mechanisms behind CPP/cargo nanocomplexes. Tartu, 2016, 147 p.
31. **Age Utt**. Role of alphavirus replicase in viral RNA synthesis, virus-induced cytotoxicity and recognition of viral infections in host cells. Tartu, 2016, 183 p.
32. **Veiko Vunder**. Modeling and characterization of back-relaxation of ionic electroactive polymer actuators. Tartu, 2016, 154 p.
33. **Piia Kivipõld**. Studies on the Role of Papillomavirus E2 Proteins in Virus DNA Replication. Tartu, 2016, 118 p.
34. **Liina Jakobson**. The roles of abscisic acid, CO_2, and the cuticle in the regulation of plant transpiration. Tartu, 2017, 162 p.
35. **Helen Isok-Paas**. Viral-host interactions in the life cycle of human papillomaviruses. Tartu, 2017, 158 p.
36. **Hanna Hõrak**. Identification of key regulators of stomatal CO_2 signalling via O_3-sensitivity. Tartu, 2017, 260 p.
37. **Jekaterina Jevtuševskaja**. Application of isothermal amplification methods for detection of *Chlamydia trachomatis* directly from biological samples. Tartu, 2017, 96 p.
38. **Ülar Allas**. Ribosome-targeting antibiotics and mechanisms of antibiotic resistance. Tartu, 2017, 152 p.
39. **Anton Paier**. Ribosome Degradation in Living Bacteria. Tartu, 2017, 108 p.
40. **Vallo Varik**. Stringent Response in Bacterial Growth and Survival. Tartu, 2017, 101 p.

41. **Pavel Kudrin**. In search for the inhibitors of *Escherichia coli* stringent response factor RelA. Tartu, 2017, 138 p.
42. **Liisi Henno**. Study of the human papillomavirus genome replication and oligomer generation. Tartu, 2017, 144 p.
43. **Katrin Krõlov**. Nucleic acid amplification from crude clinical samples exemplified by *Chlamydia trachomatis* detection in urine. Tartu, 2018, 118 p.
44. **Eve Sankovski**. Studies on papillomavirus transcription and regulatory protein E2. Tartu, 2018, 113 p.
45. **Morteza Daneshmand**. Realistic 3D Virtual Fitting Room. Tartu, 2018, 233 p.
46. **Fatemeh Noroozi**. Multimodal Emotion Recognition Based Human-Robot Interaction Enhancement. Tartu, 2018, 113 p.
47. **Krista Freimann**. Design of peptide-based vector for nucleic acid delivery in vivo. Tartu, 2018, 103 p.
48. **Rainis Venta**. Studies on signal processing by multisite phosphorylation pathways of the *S. cerevisiae* cyclin-dependent kinase inhibitor Sic1. Tartu, 2018, 155 p.
49. **Inga Põldsalu**. Soft actuators with ink-jet printed electrodes. Tartu, 2018, 85 p.
50. **Kadri Künnapuu**. Modification of the cell-penetrating peptide PepFect14 for targeted tumor gene delivery and reduced toxicity. Tartu, 2018, 114 p.
51. **Toomas Mets**. RNA fragmentation by MazF and MqsR toxins of *Escherichia coli*. Tartu, 2019, 119 p.
52. **Kadri Tõldsepp**. The role of mitogen-activated protein kinases MPK4 and MPK12 in CO_2-induced stomatal movements. Tartu, 2019, 259 p.
53. **Pirko Jalakas**. Unravelling signalling pathways contributing to stomatal conductance and responsiveness. Tartu, 2019, 120 p.
54. **S. Sunjai Nakshatharan**. Electromechanical modelling and control of ionic electroactive polymer actuators. Tartu, 2019, 165 p.
55. **Eva-Maria Tombak**. Molecular studies of the initial amplification of the oncogenic human papillomavirus and closely related nonhuman primate papillomavirus genomes. Tartu, 2019, 150 p.
56. **Meeri Visnapuu**. Design and physico-chemical characterization of metal-containing nanoparticles for antimicrobial coatings. Tartu, 2019, 138 p.
57. **Jelena Beljantseva**. Small fine-tuners of the bacterial stringent response – a glimpse into the working principles of Small Alarmone Synthetases. Tartu, 2020, 104 p.
58. **Egon Urgard**. Potential therapeutic approaches for modulation of inflammatory response pathways. Tartu, 2020, 120 p.
59. **Sofia Raquel Alves Oliveira**. HPLC analysis of bacterial alarmone nucleotide (p)ppGpp and its toxic analogue ppApp. Tartu, 2020, 122 p.
60. **Mihkel Örd**. Ordering the phosphorylation of cyclin-dependent kinase Cdk1 substrates in the cell cycle. Tartu, 2021, 228 p.
61. **Fred Elhi**. Biocompatible ionic electromechanically active polymer actuator based on biopolymers and non-toxic ionic liquids. Tartu, 2021, 140 p.

62. **Liisi Talas**. Reconstructing paleo-diversity, dynamics and response of eukaryotes to environmental change over the Late-Glacial and Holocene period in lake Lielais Svētiņu using sedaDNA. Tartu, 2021, 118 p.
63. **Livia Matt**. Novel isosorbide-based polymers. Tartu, 2021, 118 p.
64. **Koit Aasumets**. The dynamics of human mitochondrial nucleoids within the mitochondrial network. Tartu, 2021, 104 p.
65. **Faiza Summer**. Development and optimization of flow electrode capacitor technology. Tartu, 2022, 109 p.
66. **Olavi Reinsalu**. Cancer-testis antigen MAGE-A4 is incorporated into extracellular vesiclesand is exposed to the surface. Tartu, 2022, 130 p.
67. **Tetiana Brodiazhenko**. RelA-SpoT Homolog enzymes as effectors of Toxin-Antitoxin systems. Tartu, 2022, 132 p.
68. **Georg-Marten Lanno**. Development of novel antibacterial drug delivery systems as wound scaffolds using electrospinning technology. Tartu, 2022, 175 p.
69. **Liubov Cherkashchenko**. New insights into alphaviral nsP2 functions. Tartu, 2023, 171 p.
70. **Kristina Kiisholts**. Peptide-based drug carriers and preclinical nanomedicine applications for endometriosis treatment. Tartu, 2023, 138 p.
71. **Kai Rausalu**. Alphaviral nsP2 protease: From requirements for functionality to inhibition. Tartu, 2023, 175 p.
72. **Laura Sandra Lello**. Unraveling the intricate nature of the alphavirus RNA replicase. Tartu, 2023, 219 p.
73. **Houman Masnavi**. Visibility Aware Navigation. Tartu, 2023, 180 p.
74. **Kadir Aktas**. Cosmic Ray Tomography based Object Reconstruction and Recognition. Tartu, 2023, 104 p.
75. **Egils Avots**. Brain abnormality detection using statistical analysis of individual structural connectivity networks and EEG signals. Tartu, 2023, 223 p.
76. **Sainan Wang**. Structure-guided insights into the functions of CHIKV nsP2. Tartu, 2024, 154 p.
77. **Anneli Samel**. Unveiling the characteristics of cancer-testis antigen MAGEA10. Tartu, 2024, 136 p.